REPORT DOCUMENTATION PAGE

Form Approved
OMB No. 0704-0188

1. Agency Use Only (Leave blank).	2. Report Date.	3. Report Type and Dates Covered.
	4/1/84-3/31/87	Final

4. Title and Subtitle.
Bioluminescence Bathyphotometer for Naval Oceanographic Use

5. Funding Numbers.
Program Element No. 63704N
Project No. R0118
Task No. 300
Accession No. DN496415

6. Author(s).
J. Case, E. Widder, and D. Cook

7. Performing Organization Name(s) and Address(es).
University of California, Santa Barbara
Marine Sciences Institute
Santa Barbara, Ca 93106

8. Performing Organization Report Number.
CR N00014-84-C-0604

9. Sponsoring/Monitoring Agency Name(s) and Address(es).
Naval Ocean Research and Development Activity
Code 311
SSC, MS 39529-5004

10. Sponsoring/Monitoring Agency Report Number.

11. Supplementary Notes.

12a. Distribution/Availability Statement.
Approved for public release distribution is unlimited.

12b. Distribution Code.

13. Abstract *(Maximum 200 words).*

14. Subject Terms.
bioluminescence, bilogical oceanography, optics, biochemistry

15. Number of Pages.
59

16. Price Code.

17. Security Classification of Report.	18. Security Classification of This Page.	19. Security Classification of Abstract.	20. Limitation of Abstract.
Unclassified	Unclassified	Unclassified	

BIOLUMINESCENCE BATHYPHOTOMETER FOR NAVAL OCEANOGRAPHIC USE

FINAL REPORT

Submitted by: James F. Case, Edith A. Widder, and David P. Cook, Marine Sciences Institute, University of California, Santa Barbara, CA 93106

This is the final report as required, summarizing all work accomplished under NORDA contract N00014-84-C-0604, dated 4/1/84-3/31/87 inclusive.

I. PROJECT REPORT-SUMMARY

The recently completed contract has resulted in the development and proof of a new concept in bathyphotometry for measurement of in situ bioluminescence, incorporating several novel improvments in system control and calibration, hydrodynamic excitation, data transfer and storage, and bioluminescent particle counting.

In summary, the bathyphotometer system (hereinafter referred to as HIDEX-1 BPS, for High Intake Defined EXcitation BathyPhotometer System) developed at UCSB is composed of four interactive subsystems: (1) the bathyphotometer subsystem (2) the CTD subsystem, (3) the deployment subsystem, (4) and the shipboard computer subsystem.

The bathyphotometer subsystem (~~Figs. 1-2, Fig. 6~~) is basically a long tube composed of an intake section, a detector section, a thruster section, and an exhaust section. The intake section has a hydrodynamically designed nosecone and stimulus screen, followed by an optical wedge and fiber optic array for bioluminescent particle counting. The detector section of HIDEX-1, which also includes part of the intake section, is composed of white PVC tubing with alternating fiber-optic triplets arrayed longitudinally. The thruster section is a stainless-steel expansion cone flanged to the detector section, having within a coaxially mounted 1/3 HP, DC motor magnetically coupled to a propeller which supplies the thrust for the high flow rates obtainable with this system. The exhaust section incorporates a helical light baffle to block down-welling light. Power and electronics for control and operation of the subsystem is incorporated in two pressure housings mounted external to the bathyphotometer.

The CTD subsystem, a commercially available unit manufactured by InterOcean Systems, supplies HIDEX-1 with information on conductivity, temperature, and depth of the surrounding seawaters, as well as X and Y axis tilt data.

The deployment subsystem consists of a commercially available portable winch (InterOceans Systems, Inc.), spooled with 600

meters of double-armored coaxial cable, a cable sheave suitable for attachment to a ship's A-frame or crane, and a stainless steel cage which incorporates within its structure the CTD, pressure housings, and the bathyphotometer.

The shipboard computer subsystem is comprised of a Compaq 386 microcomputer, printer/plotter for hard copy, bulk data storage device, and power supplies and interface unit. All mechanically sensitive units are shock-mounted in two shipping containers, which can be interlocked at sea and used as operating consoles.

After deployment of the bathyphotometer, a controlled vertical descent of the instrument is maintained, while bioluminescence data , CTD and tilt data, and system status data are acquired by the appropriate sensors, digitized, and transmitted to the topside computer system for analysis, storage and display. The HIDEX-1 BPS allows the operator to control various parameters of the subsytems via menu-driven software displayed on a color monitor. System commands, which can be altered at any time by the operator in ManualMode, are made by means of standard keyboard entry. Under operator control are thruster speed (and concomitantly, flow rate and volume), photomultiplier sensitivity, photomultiplier gain, real-time data analysis, graphics display mode, vertical deployment rate, and data storage and retrieval. Provisions are also made for standard set-up files to enable the operator to preset parameters. Thereafter a vertical, bioluminescence profile may be run with a single keystroke (AutoMode).

II. PROJECT REPORT-DETAIL

A. Summary Specifications

As required in the specifications set forth by Code 311, NORDA (K.M. Ferer, Program Manager), this newly developed vertical profiling bathyphotometer:

1. Is under computer control with real-time readout of critical information and disc storage of all data for rapid and convenient recovery and analysis.

2. Is self-contained, requiring only ship's power and a crane or A-frame for deployment.

3. Excites bioluminescence in a hydrodynamically defined fashion which allows quantitative conversion of total stimulabule light (TSL) from the bathyphotometer for use in models of bioluminescent sources under development within the Navy.

4. Samples at a sufficiently high rate to
   a. effectively sample all types of bioluminescent sources, including the larger zooplankton now considered as possible major contributors to oceanic BL, and

   b. obtain robust statistical evaluations of TSL as a

function of depth in durations of time brief enough not to interfere with ship operations.

It should be noted that original specifications were developed with another contractor. At the time of our undertaking the project, only the basic hydrodynamic design had been defined. At UCSB, modifications were made to the original design when we assumed contractural responsibility and, subsequently, as the project developed. At UCSB, the entire electronic design, deployment system, instument packaging, and software and computer system was developed and fabricated. Substantial modifications were also made to the system detector chamber, including the decision to utilize a unique, distributed fiber-optic integrated light detection method.

B. Description of HIDEX-1 BPS

The HIDEX-1 BPS (Figs. 1-2) is a vertical profiling survey bathyphotometer designed to measure bioluminescence potential of the water column to depths of 400 meters (design depth 500 meters) in absolute units of photons per second per unit volume (intensity), or in photons per volume (total flux), from a statistically significant volume with a calibrated hydromechanical stimulus.

1. INLET-INITIAL SECTION: (Figs. 2-3) In order to maintain initial laminar flow the nose cone of the BP was designed to effect transition of zero to maximum flow with a minimum turbulence at the inlet, and poured from urethane polymer to reduce weight and supply a high resistance to corrosion and abrasion. The inlet size of 12.7 cm diameter exceeds previous BP inlet diameters by more than 25 times, and permits high pumping rates (Fig. 3, Table 1). Flow entering the nosecone immediately impacts the stimulus screen inserted at the upsteam end of the intake section, generating a hydrodynamically defined turbulence (see Appendix A for detailed analysis), which in turn stimulates bioluminescence from entrained organisms. Three mesh sizes of stimulus screens (1 cm X 1 cm, 2 cm X 2 cm, 4 cm X 4 cm grid size) have been fabricated to be easily interchangable under field conditions.

2. INLET-DETECTOR AND DIODE SECTION: Immediately after the stimulus screen, the flow enters a 9 cm section of the inlet (Fig. 4,) which contains the first fiber optic triplet of the integrating array and a photodiode which is the first in a series of 8 photodiodes equally spaced down the combined length of the inlet section and the detector section of the BP. The photodiode octet senses the "standing wave" of bioluminescence within the BP (Fig. 5), which information is displayed graphically to the operator. Such information can be used to adjust flow rates so the decay of the bioluminescence falls to zero at the end of the detector section (insuring maximal light capture within the chamber; ie, no ejection of bioluminescing organisms from the chamber and no dark volume). Photodiode information is also used by system software to calculate e-folding (decay kinetics of the

bioluminescence), which can be used in conjunction with data from the luminescent particle counter (ring counter) to identify population changes during the vertical profile. E-folding data also enables calculation of photons per second per volume.

A ninth diode is mounted in a separate pressure housing outboard of the BP, and serves to monitor upwelling light for background correction of the of the bioluminescence detected by the PMTs. Input to the diode can be occluded, in which case the output of the diode can be used to correct for "dark current" in the remaining 8 diodes.

3. INLET-RING COUNTER SECTION: 9 cm downstream of the stimulus screen the flow passes through the ring counter (Fig. 4, Figs. 6-7), a lensing system whereby the acceptance angle of a 31 fiber optic radial array is narrowed from 44 degrees to 7 degrees, longitudinally, and expanded to 54 degrees laterally. Bioluminescent organisms passing the ring counter are detected as single particles by this optical system and its associated PMT, and the data is sent to the topside computer system for display and analysis. Gain and sensitivity of the PMT is remotely controllable from the surface.

4. DETECTOR SECTION: The detector chamber of HIDEX-1 is an integrating cylinder (96 cm X 12.7 cm ID - FIG. 4) constructed of white PVC, designed to maximize light gathering efficiency while reducing bias due to an organism's orientation, a critical consideration with zooplankton owing to the fact that their light emission is frequently highly directional. The length of the chamber was designed to produce a residence time sufficiently long enough to measure the total light output from a single dinoflagellate flash at the maximum pumping rate. Measuring volume of the chamber is 16 liters. Integrated light detection is by means of 96 fiber optics (AMP, 1 mm multimode plastic fibers) arranged in alternating inverted triplets longitudinally along the chamber and inlet section. The geometry of this arrangement results in a minimally overlapping array of light capture cones, providing 90 % coverage of the integrating cylinder. Fibers are mounted with quick-change "Ultratorr" fittings so that each fiber can be individually replaced. Bundled fibers transmit integrated bioluminescence to a side window PMT via a polycarbonate window located in a pressure housing. The PMT detector surface is itself positioned within an integrating spheroid to further reduce positional bias of sources and increase sensitivity of the system. As in the ring counter, gain and sensitivity of the PMT is controllable from the surface.

The detector chamber has been modified to accept a second stimulus screen centered along its length. This allows greater latitude for experimental control of spatial and temporal intensity of the hydrodynamic stimuli for differing populations of organisms resident in the scattering layers.

5. THRUSTER SECTION: This section consists of a 43 cm stainless steel expansion cone designed to effect a smooth transition of

the flow from the detector chamber to the exhaust section of the BP. A 1/3 HP thruster (Giannini PetroMarine) is mounted coaxially within the housing. The thruster has been extensively modified to allow precise remote control of RPM in a closed loop system.

6. EXHAUST SECTION: A 28 cm X 20.3 cm ID section of grey PVC terminates the BP. Mounted within the circumference of the exhaust section is a 1 1/2 turn helical light baffle which shields the detector section from downwelling light.

C. System Hydrodynamics

1. Flow Dynamics: Flow through the detection chamber is induced by a 1/3 HP, 20 lb DC thruster motor (Gianinni PetroMarine). Motor RPM and power use is monitored in real time at the surface. Motor speed and thereby flow velocity are under operator control. The motor can be reversed to clear blockages. Motor and impeller design are shown in Fig. 8.

Laminar flow is maintained through the BP until the onset of turbulence at the excitation screen. Turbulence is generated with a defined geometry and for a defined distance downstream of the excitation grid. Sheer forces within the turbulent field stimulate bioluminescence emission from organisms resident within the water column. Maximal stress is exerted at the screen and little additional stress is imposed throughout the remainder of the detection chamber (Appendix A). Consequently, excitation is well defined and localized, as compared with other bathyphotometers, and prestimulation of the organisms prior to screen excitation is minimized by the entry design (Figs. 1-3).

2. Capture Volume: The maximum pumping rate of 2400 liters/min produces an effective cone-shaped capture volume immediately ahead of the inlet of 11,300 cc. This "lethal cone" extends for 300 cm for organisms with escape velocities less than or equal to 10 cm/sec. This is greater than a 1000% improvement over pre-existing designs (Table 1), permitting high capture efficiencies without species bias since the maximal escape speed reported for most organisms of interest is about 25 cm/sec and most are at 10 cm/sec or less.

D. System Calibration (Fig. 9)

1. Radiometric Calibration: Instrument output is fully intercalibrated in terms of photons per second per unit volume. Three calibration procedures are used and intercompared:

a. Static calibration: C^{14} phosphor rods (in-house design and calibration) used as secondary standards. These are suspended on axis in the detector chamber as a fixed and uniform photon source, yielding a direct measurement of absolute number of photons. Geometric quantum efficiency and integration efficiency of the detector chamber are also obtainable with this method.

b. Dynamic calibration: Spherical C^{14} phosphors (in-house design

and calibration) used as secondary standards. These are entrained in the flow and pass through the detector section as organisms would. This procedure gives a direct measure of statistical variability of sampling and the relationship between instrument readout and absolute number of photons. Event capture efficiency of the ring counter can also be obtained.

c. Bioluminescence bacteria transfer standard: The Lee calibrated photometer and bioluminescent bacteria transfer standards have recently been received. We are in the process of comparing these with the other methods used.

d. Biological calibrations: Cultured dinoflagellates (Pyrocystis) are measured in an integrating sphere for total stimulable light (TSL) per cell. An aliquot of cells is counted microscopically for each calibration series. Samples of a known concentration and TSL are run concurrently in HIDEX-1. The resulting comparison of the photon yield defines a transfer function relating the calibrated BP data with TSL.

E. System Design And Operation

1. Mechanical Design: The BP and all ancillary equipment are contained within a 106 X 106 X 285 cm cage of 2.5 cm stainless tubing (0.305 cm wall thickness), designed to protect vital components against shock-loading from all directions (Figs. 1-2). Control commands and system power are supplied to the BP by an electrical and load-bearing connector via a double-armored coaxial cable, coupled to a four-point suspension harness attached to the exhaust section of the cage. Control of descent and depth are managed from the surface using an InterOcean Model 1673-3-LW winch, equipped with a level wind and modified to allow quick-change of the entire spool and cable at sea (Fig. 10). Digitized data and system status readouts are sent to the surface computer and control system on the coax center conductor. System power to subsurface components is impressed across the coax shield and center conductor concurrent with the data stream.

2. Electronics (see Appendix B): With the exception of the CTD and diode system, the electronics are contained in two 20 cm X 75 cm cylindrical pressure housings, PH-1 and PH-2., mounted on opposite sides of the system cage and centered over the detector section (Figs.1-2). The integrated light and photoevent data are led from the detector chamber and ring counter of the bathyphotometer by bundled optic fibers to PH-1, which contains the PMTs for TSL and photoevent counting, and the associated electronics for control of power, sensitivity, and gain. PH-2, the second of the two pressure housings, contains system power supplies, filters, motor power and control circuitry, data communication circuitry for D/A and A/D conversion and transmission of the data stream, and the CPU which controls subsurface functions. After appropriate conditioning, signals from system status monitors, motor functions, bioluminescence, and photodiode readouts are brought together in PH-2 for transmission to the surface on the center conductor of the

coaxial cable.

3. S4-CTD System (see Appendix B): The conductivity, temperature, and depth sensor, a self-contained unit manufactured by InterOcean, is equipped with rugged tungsten probes for the CTD monitoring and an internal flux-gate magnetometer for two dimensional x-y tilt data (Fig. 11). All components of the system are housed in a 25 cm glass-reinforced polymer sphere, neutrally bouyant in seawater, and deployable to 1000 meters. HIDEX-1 supplies power for the CTD. Analog signals from the CTD are transferred to PH-2 (electronics pressure housing) for digitizing and incorporation into the outgoing data stream.

4. Data Handling: HIDEX-1 BPS is capable of rapid data reduction and analysis. The surface computer system displays bioluminescent data and system status readouts in real time during vertical profiling. Environmental data, including conductivity, temperature, depth, and tilt are recorded during profiles and are available for display on demand. Bioluminescence data in absolute photons can be plotted as a function of depth, in conjunction with temperature and salinity, or as a function of either of these parameters. Data sampling rate (256 kilobaud/sec) allows expansion of areas of interest to reveal small scale detail.

5. Deployment: HIDEX-1 BPS is portable aboard any vessel which has the capability of craning aboard packages that do not exceed 700 lbs and whose linear dimensions do not exceed 3.5 m X 3.5 m X 7.0 m. The system is deployable from the deck of any vessel having a minimum linear space and maximum crane or A-frame height, such that the angle of the winch cable and the deck is less than 20 degrees to insure a minimum of cable strain during spooling. Vessels selected for deployment must be able to supply HIDEX-1 BPS with 208-220 vac, 10 amp single phase for winch operation, and 115-120 vac, 10 amp clean and stable 60 cycle power for system power.

6. Operational Results: In November 1986, HIDEX-1 BPS was first deployed aboard the RV New Horizon out of Scripp's Institute of Oceanography (SIO - San Diego, CA) for system test and evaluation. Data acquired during this shakedown cruise is included in this report as Figs. 12-16.

Following the SIO cruise, HIDEX-1 was operationally tested aboard the naval research vessel deSteiger in March 1987, during a cruise in the Santa Barbara Channel. Examples of data typical of that obtained during vertical profiles are provided as Figs. 17-21.

After analysis of system operation and data from the November and March cruises, several software and hardware changes were accomplished to HIDEX-1, and the system was redeployed in August 1987 for an extended cruise aboard the RV Endeavor in the Sargasso Sea. Data typical of that obtained during this cruise is included as Figs. 22-23.

Based upon evaluation of CTD and bioluminescence data obtained from the Sargasso cruise, several modifications to HIDEX-1 are contemplated, pending approval of changes and funding. These include the addition of a fluorimeter, a transmissometer, an improved thruster, a strobed CCD (charge-coupled device) camera for particle counting, and improved light baffling for operation at higher latitudes.

Figure 1

A. Lateral view of HIDEX-1 BPS. Major components of the system are labeled.

B. Front and rear views of HIDEX-1 showing location of pressure housings, PH-1 and PH-2. Radial placement of components are readily apparent in this view.

Figure 2

Multiple views of HIDEX-1. Three dimensional aspect allows the viewer to obtain a sense of scale and complexity of the instrument.

Figure 3

Inlet size comparisons for HIDEX-1 and APL towed BP. Flow turbulence at the inlet of HIDEX-1 is minimized by the inlet and nosecone design.

Figure 4

Longitudinal view of detector chamber and thruster showing detail of inlet section and ring counter at left of figure. The ring counter (bioluminescent particle counter) consists of a surface-silvered Plexiglass annulus radially arrayed with 31 optic fibers, which detects bioluminecent particles passing through a narrow (7 degrees) field of view, and relays the optical data to the surface computer via PMT-2. Detail of fiber optic mount and photodiode array are also indicated.

Figure 5

Diagram of the "standing wave" of bioluminescence within the detector chamber downstream of the stimulus grid (arrow). In calculating e-folding (exponential decay) of the bioluminescence, tau is a measure of the time for 1/e decay of the light residing within the chamber.

Figure 6

Detail of the ring counter showing lateral and cross-sectional views of optical wedge.

Figure 7

Field of view analysis of the ring counter. The upper graph shows the response of the detector to a point source of light moved radially within the 54 degree field of view of the detector. The response is remarkably constant throughout the field.

Moving the point source longitudinally (upsteam to downstream) through the narrow - 7 degree - field of the detector yields a response that decays rapidly within a short distance of the wedge (lower figure).

Figure 8

HIDEX-1 thruster. Motor power is magnetically coupled to the the hub shaft (see detail), obviating the need for shaft seals.

Figure 9

Radiometric calibration of the bathyphotometer (upper figure) is effected using C^{14} phosphor rods within the detector chamber and comparing the result to that obtained using smaller rods of known output in the integrating sphere. Spectral emission of the phosphors are shown in the insert.
A similar approach is used for bilogical calibration of the system (lower figure).

Figure 10

Deployment system - winch, control box and cable. Future plans call for computer control of deployment, allowing a single operator to run the system once the bathyphotometer is submerged.

Figure 11

InterOcean Model S4-CTD. The unit for HIDEX-1 was modified to delete the battery pack, on-board memory and the speed sensor, and substitute the platinum resistance thermal sensor with a response time of 60 msec.

Figures 12-16. <u>New Horizon Cruise Data</u>

12 - Background light intensity at depth. With motor speed at zero and , consequently, flow through the detector chamber at zero, the background intensity can be obtained by the system for TSL (PMT-1) and bioluminescent events (PMT-2).

13 - Stimulated light intensity at depth. With motor speed varied from 0-2500 RPM (flow 0 - 80 % maximum) the light intensity as a function of motor speed is plotted.

14 - Typical vertical bioluminescent profile obtained with HIDEX-1 BPS as a function of depth. Motor speed and conductivity are listed at the top of the figure. Time required for the profile = 300 sec.

15 - Expansion of the area of interest around the thermocline in the preceding figure. The system stores far more data than is normally plotted. The operator has the option to both expand an area of interest and increase the resolution of the display (cf Fig. 19).

16 - Plot of bioluminescent data of the previous figure as a function of temperature to demonstrate the flexibility of the system, allowing the operator great latitude in acquistion, display and analysis of data.

Figures 17-21. deSteiger Cruise Data

17 - Light intensity in photons/sec as a function of motor speed. The bathyphotometer was held at depth while motor speed was varied between 10 - 80 %. Note the added resolution of the data plot as compared with Figure 13.

18 - Vertical profiles of two casts characteristic of those obtained for the Santa Barbara Channel. Gain and voltage for PMT-1 (TSL) and flow velocity within the detector chamber are listed above the graph. Note the added resolution of the data plot as compared with Figure 14.

19 - Vertical profile data taken from PMT-2, the ring counter. High resolution available to the operator is demonstrated in the inset, which is an expansion of the minimum encircled on the lower graph.

20 - At constant motor speed, the event counter data can also be analyzed in terms of size classes, since a larger organism, on the average, moving through the narrow field of view of the counter will yield an "event" of longer duration than a smaller organism. For example, from the figure with data plotted as a histogram with size classes = 1/250 sec (4 msec), event counter data yields 740 events of 4 msec, 300 events of 8 msec, etc.

21 - Dwell time of bioluminescent organisms within the detector chamber plotted as a function of motor speed (two vertical profiles - 31 March, 1 April). Dwell time is inversley related to motor speed (and therefore flow velocity through the chamber). As the flow velocity

increases, the stimulus grid imparts a larger stimulus to the organisms. This results in an increased TSL as more of the population is optimally stimulated, peaking between 0.4 - 0.6 sec. The decrease in TSL for shorter residence times is due to ejection of the organisms from the chamber before their light output has decayed. This information, in conjunction with e-folding data, enables the operator to control motor RPM to optimize flow velocity relative to the dominant organism resident in the bioluminescent population.

Figures 22-23. Endeavor Cruise Data

22 - Vertical profile of bioluminescence for a descending and ascending cast. PMT-1 output (TSL) plotted as microwatts/steradian/cubic meter (intensity). During ascent the output of the system is lessened due to unfavorable geometry of the cage preceding the flow intake, reducing the efficiency of the capture cone.

23 - Typical vertical profile of Sargasso Sea data. Note the high surface temperature of this body of water. As is frequently found for bioluminescence, the peak signal occurs in the area of the thermocline (cf Fig. 14).

APPENDIX A

HIDEX-1 BPS hydrodynamics and flow analysis data.

APPENDIX B

Figures B-1 thru' B-5. Block diagrams of the HIDEX-1 BPS signal and power flow and system interconnects.

CHARACTERISTICS OF SOME RECENTLY DEVELOPED BBPS

(All enclosed pump types)

TYPE		SWIFT (83)	APL (84)	LOSEE (85)	NORDA (86)
FLOW	L/MIN	15	60	66	680
VELOCITY	CM/SEC	na	66	na	400
CAPTURE VOL.	CC(1)	30	500	700	4500

(1) At 10 cm/sec escape velocity

EXCITATION MECHANISM	
SWIFT (83)	PUMP IMPELLER
APL (84)	RT. ANGLE ENTRY TURBULENCE
LOSEE (85)	CONSTRICTION TURBULENCE
NORDA (86)	SCREEN

Table 1

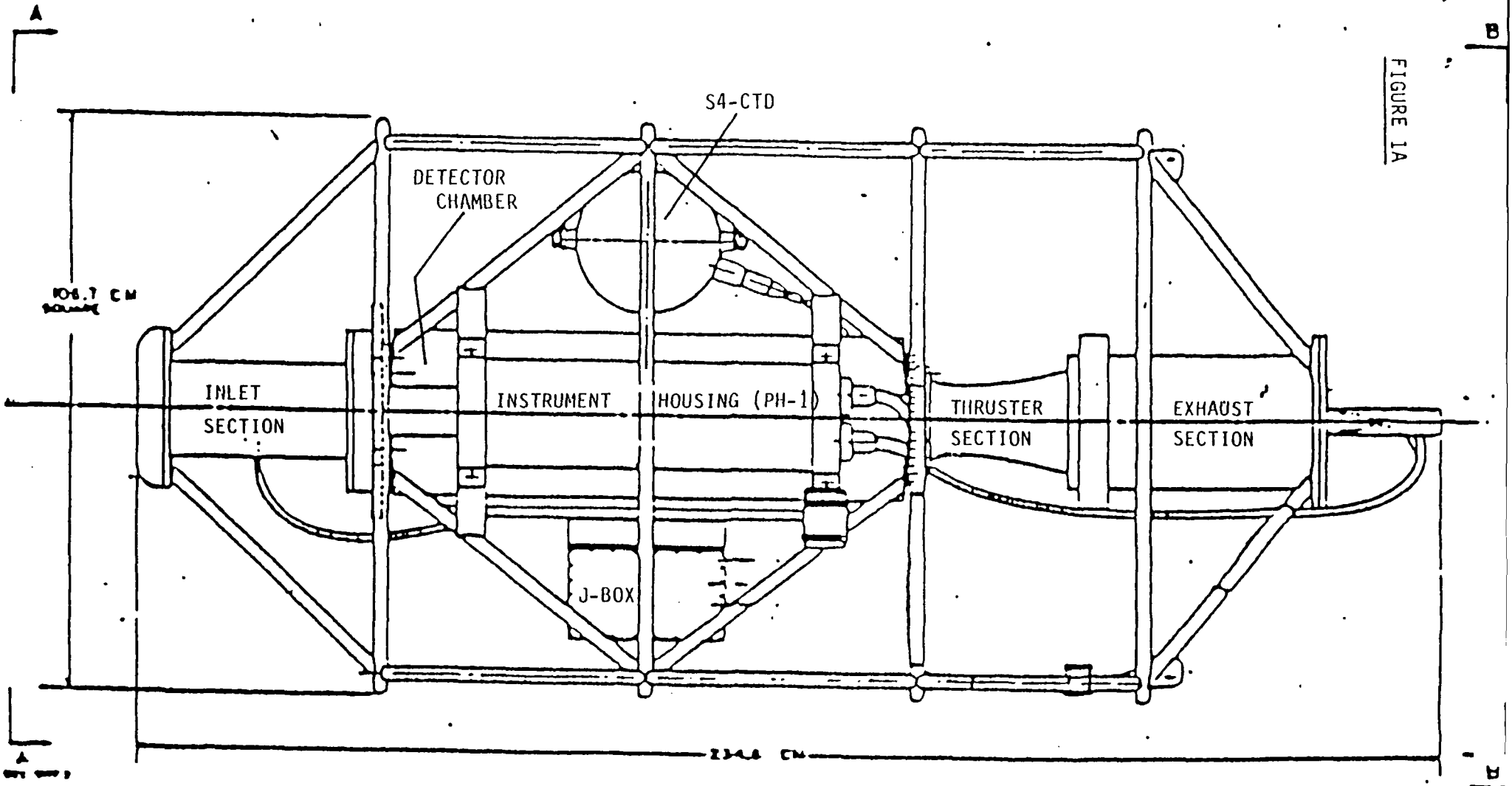
A
B
S4-CTD
DETECTOR
CHAMBER
INLET
SECTION
INSTRUMENT
HOUSING (PH-1)
THRUSTER
SECTION
EXHAUST
SECTION
J-BOX

FIGURE 1A

FIGURE 1B

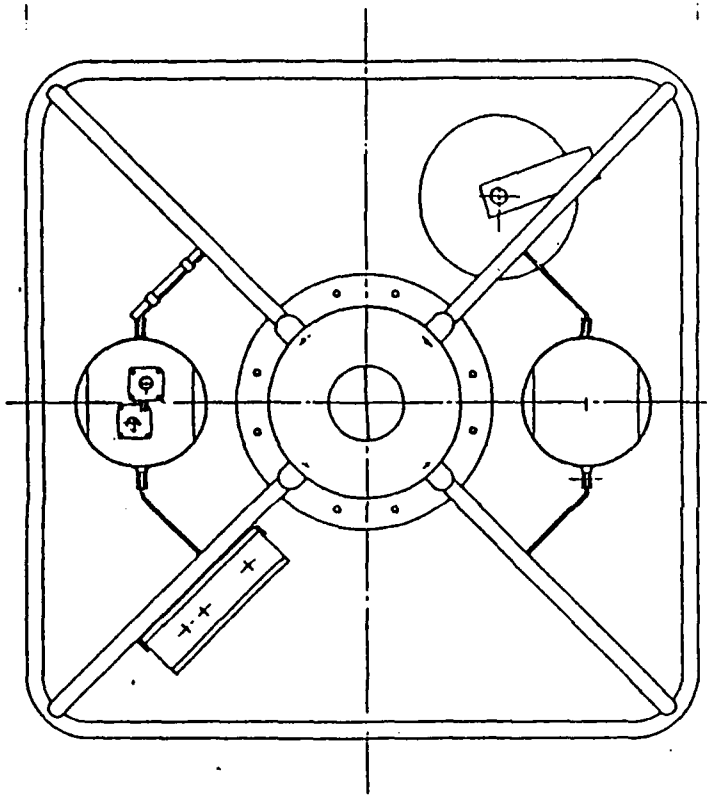

FRONT VIEW A-A

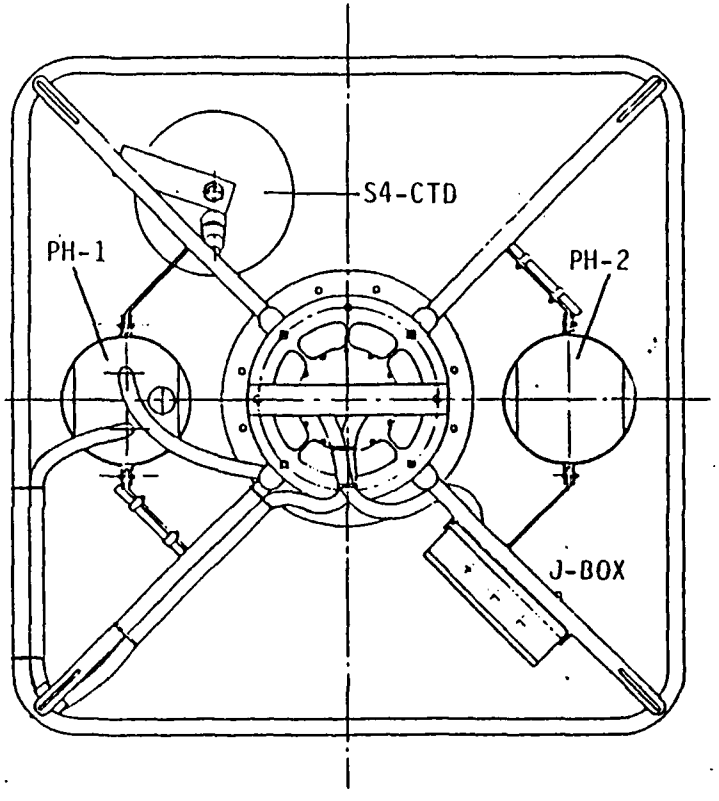

REAR VIEW B-B

NORDA BPS
UNIVERSITY OF CALIFORNIA SANTA BARBARA CA
BIOLUMINESCENCE PROFILING SYSTEM
BATHYPHOTOMETER ASSEMBLY
SHEET 2

FIGURE 2

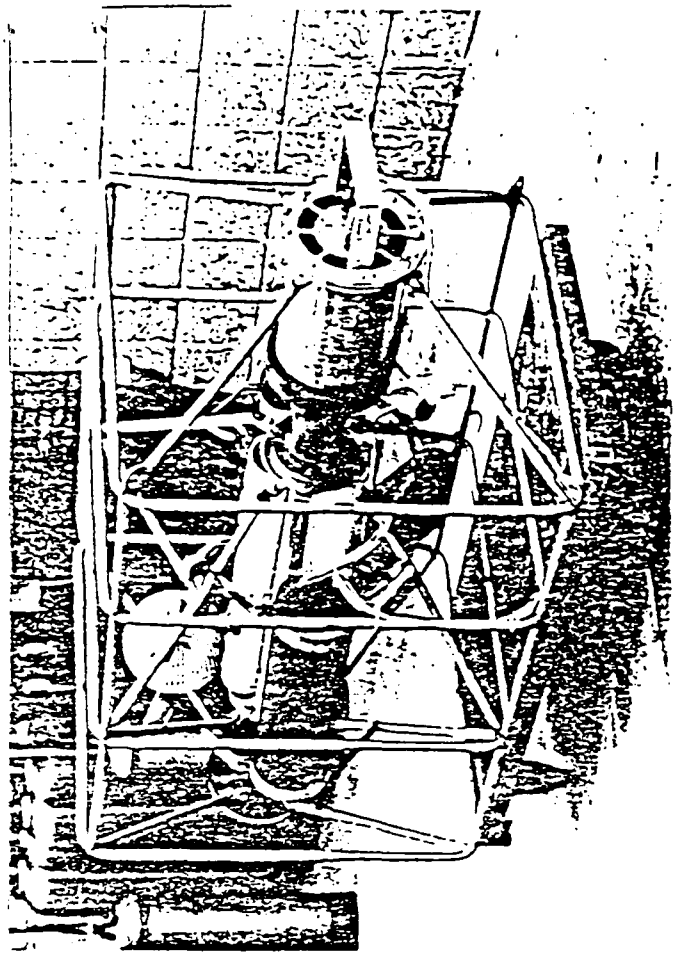

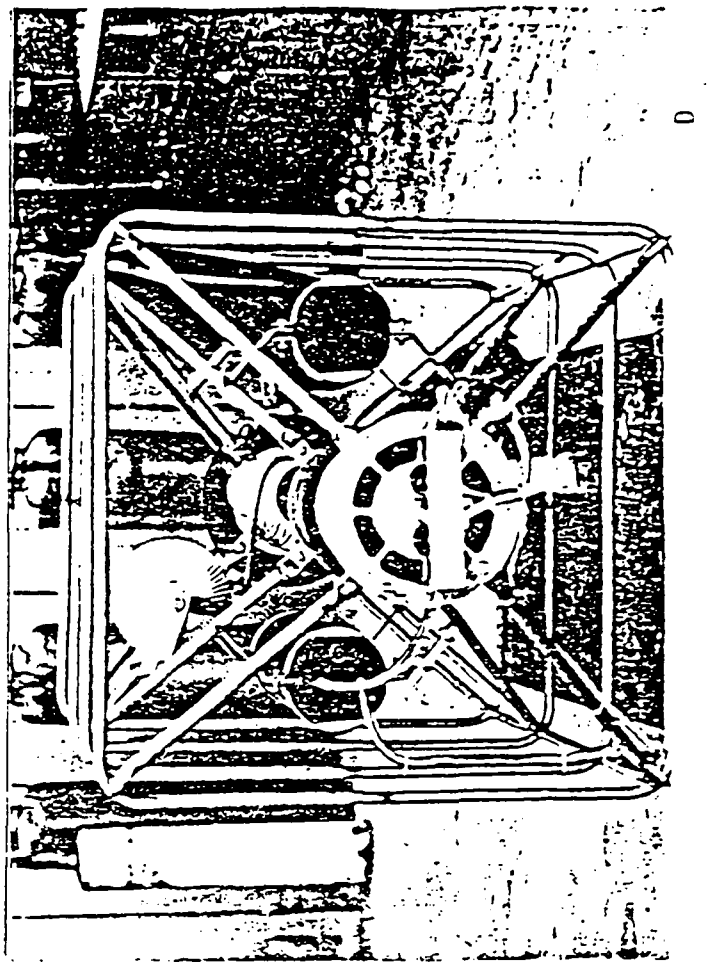

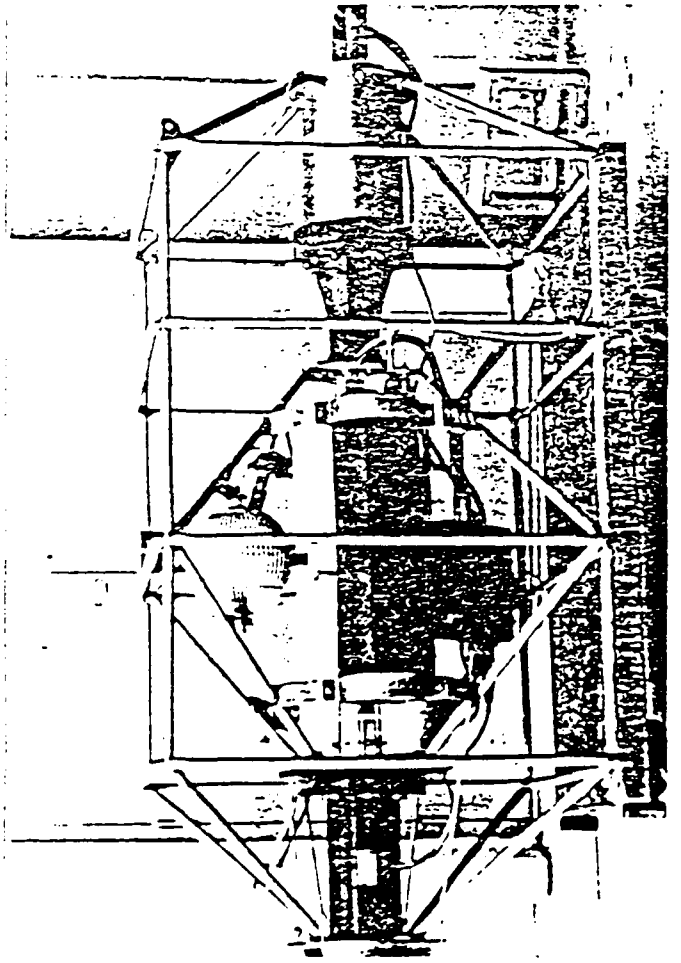

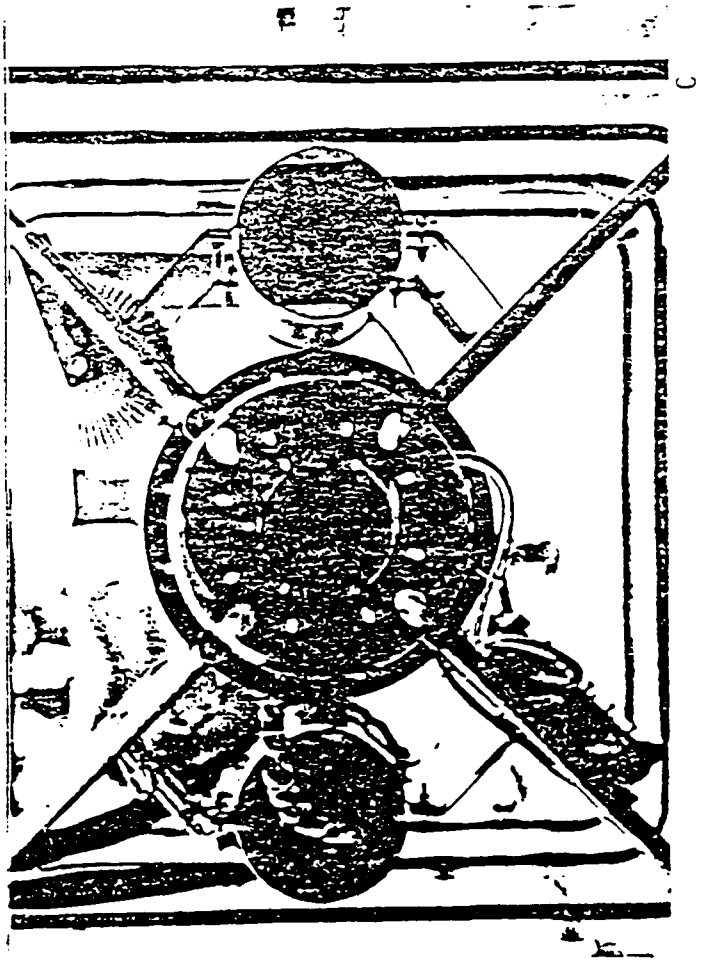

FIGURE 3

INLET SIZE COMPARISONS:
NORDA AND A TYPICAL BIOLUMINESCENCE DETECTOR

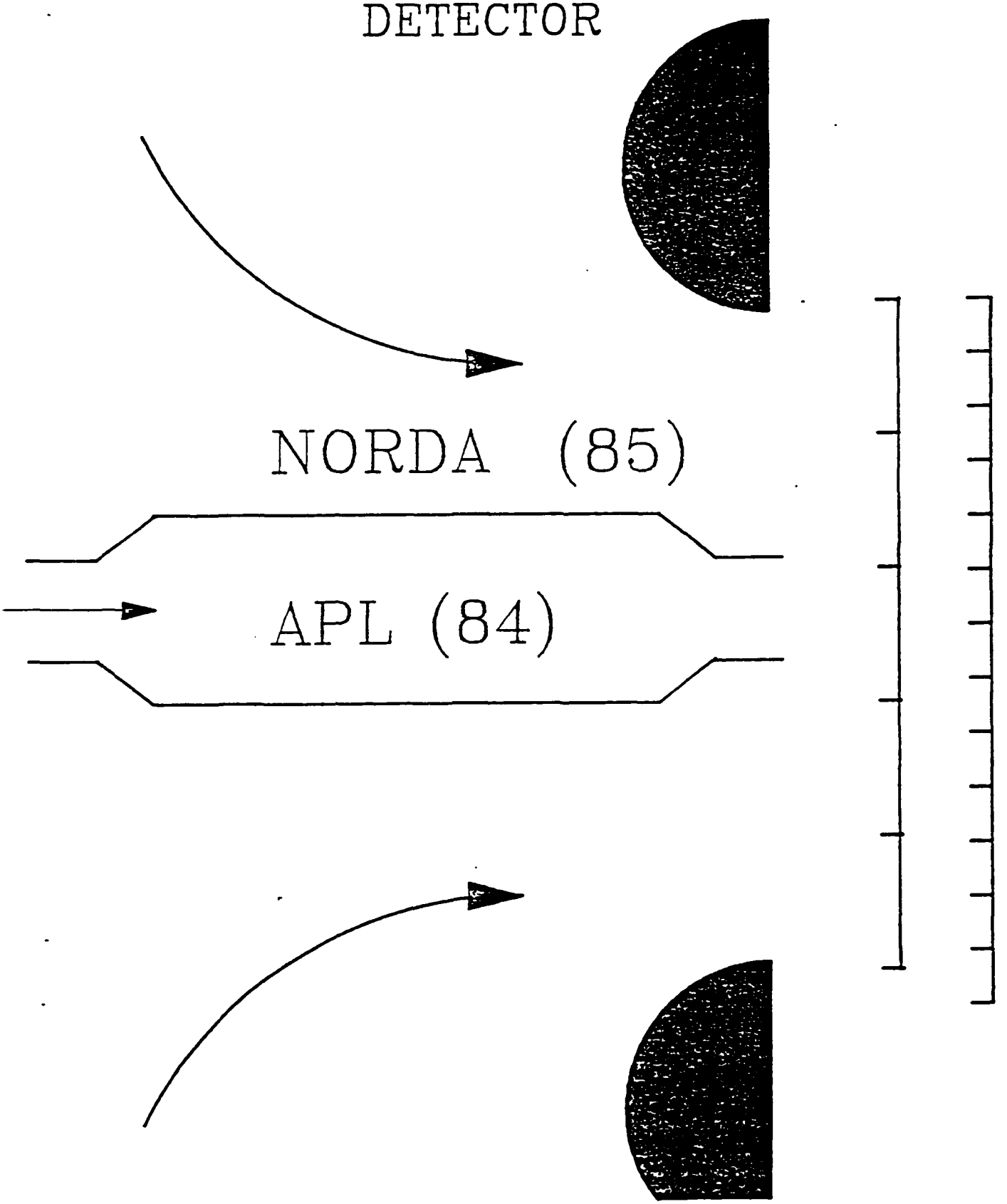

FIGURE 4

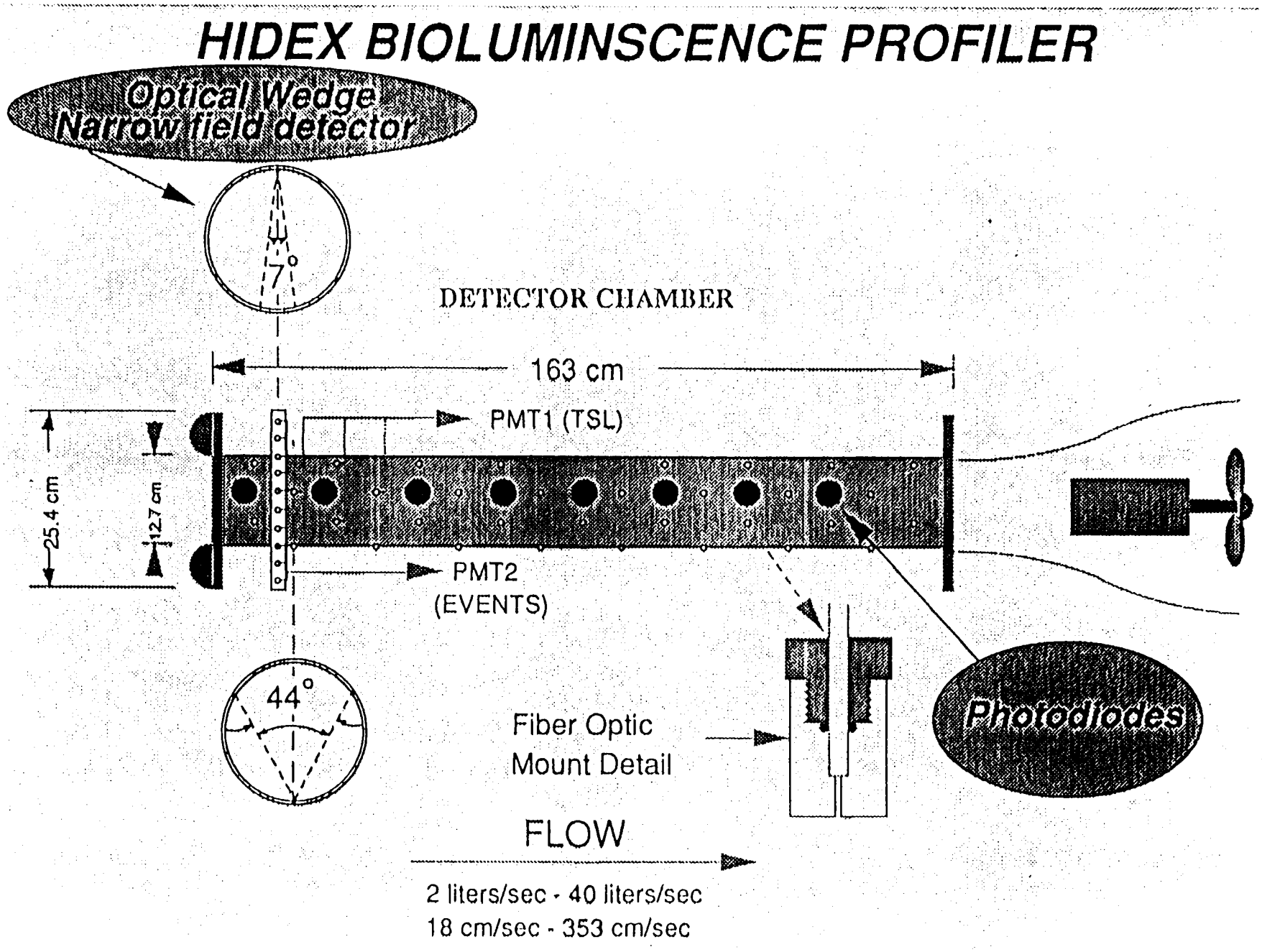
HIDEX BIOLUMINSCENCE PROFILER
Optical Wedge
Narrow field detector
7°
DETECTOR CHAMBER
163 cm
PMT1 (TSL)
25.4 cm
12.7 cm
PMT2
(EVENTS)
44°
Fiber Optic
Mount Detail
Photodiodes
FLOW
2 liters/sec - 40 liters/sec
18 cm/sec - 353 cm/sec

FIGURE 5

BP MEASUREMENTS

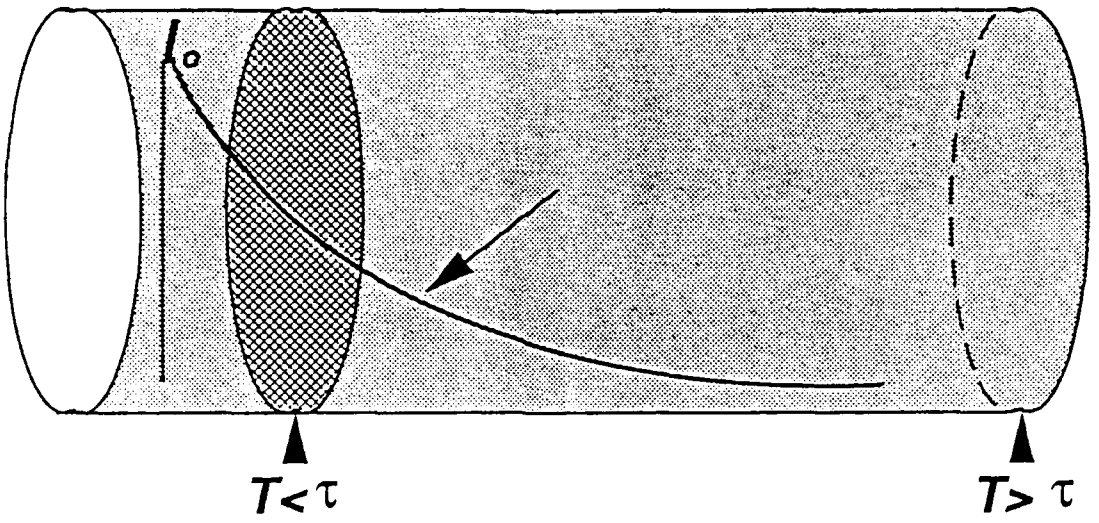

T = residence time in chamber

V = volume of chamber

n_o = no. of organisms/volume sw

Q = volumetric flow rate V/T

I_{BP} = avg intensity measured by BP

$$P_{tot\text{-}BP} = n_o V I_o \tau \ (1-e^{-T/\tau}) \quad \text{(photons)}$$

$$I_{BP} = n_o Q I_o \tau \ (1-e^{-T/\tau}) \quad \text{(photons/sec)}$$

$T > \tau \quad I_{BP} \sim n_o Q I_o \tau$

$T < \tau \quad I_{BP} \sim n_o V I_o$

$$I_{BP}/Q = n_o I_o \tau \ \text{(p/cc)}$$

$$I_{BP}/Q\,\tau = n_o I_o \ \text{(p sec}^{-1}\ \text{cc}^{-1}\text{)}$$

$$I_{BP}/V = n_o I_o \tau \ \text{(p sec}^{-1}\ \text{cc}^{-1}\text{)}$$

FIGURE 6

Optical Wedge Narrow field detector

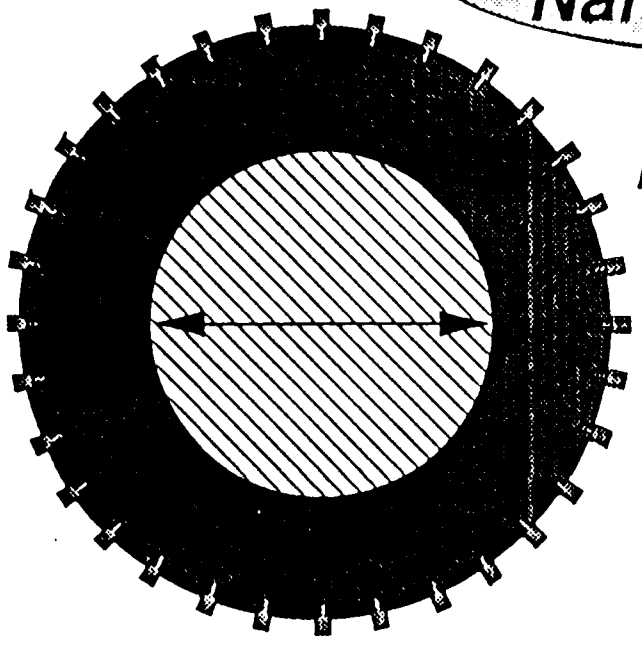

lateral view

cross section

Design features giving high resolution low signal event measurement

- *7° Longitudinal field of view*
- *54° Lateral field of view*
- *32 Fiber optics surrounding wedge coupled to PMT.*
- *Light funneling*
- *Silvered Surfaces*

FIELD OF VIEW ANALYSIS

FIGURE 7

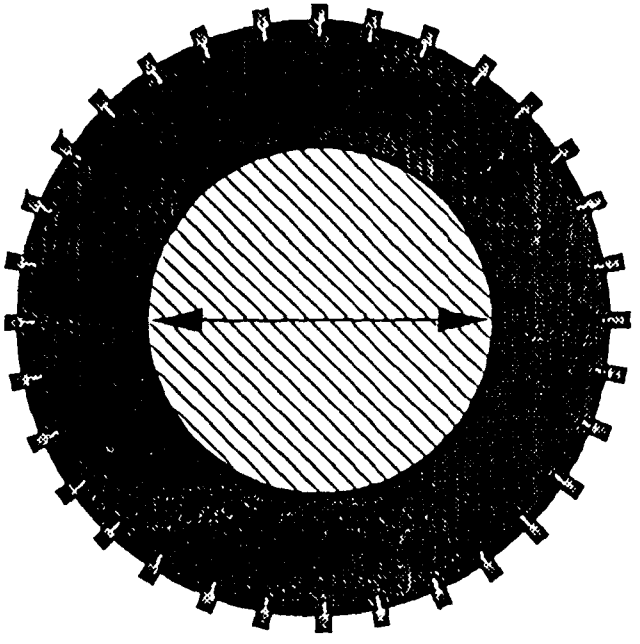

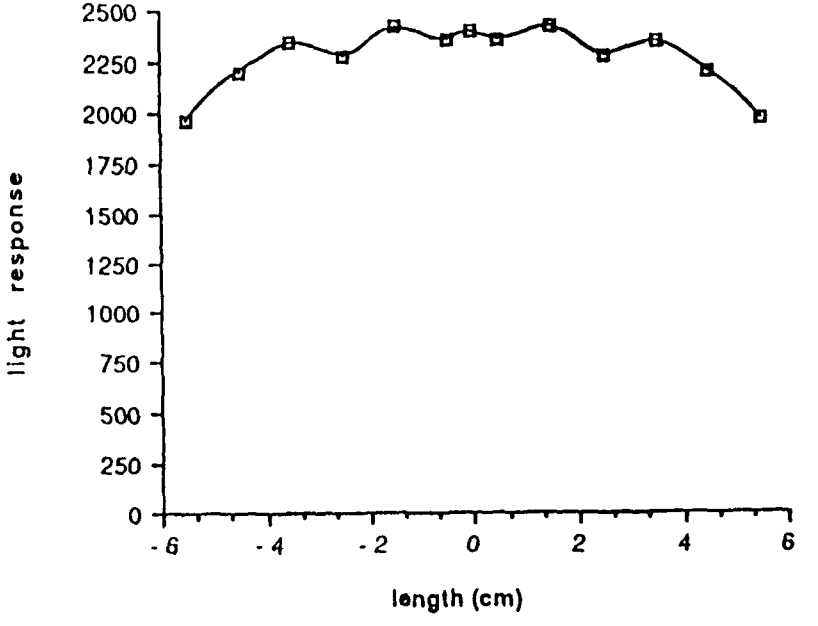

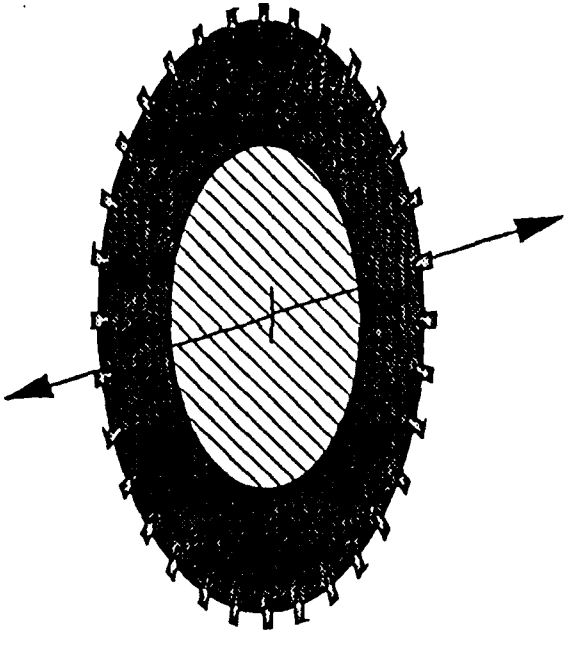

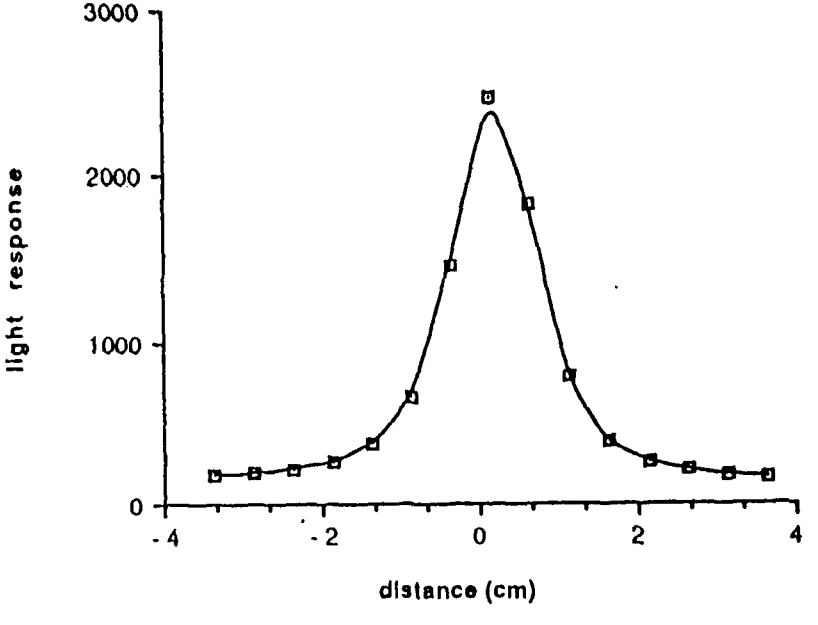

FIGURE 8

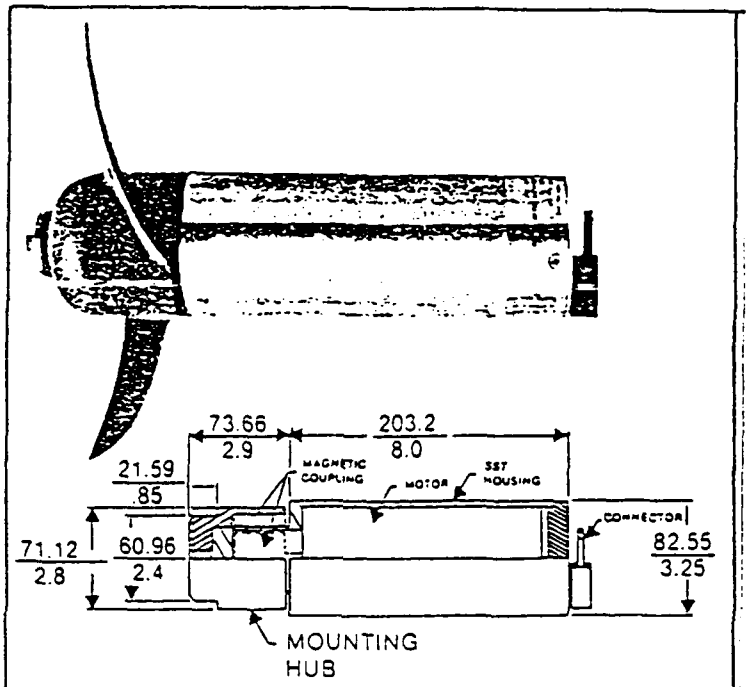

Conventional dc thruster develops 20 pounds of thrust when energized by a 120 Vdc source (2.5 A).

At depths of several thousand feet, it operates in air being totally sealed within a watertight enclosure. Torque to the propeller is transmitted through a magnetic coupling.

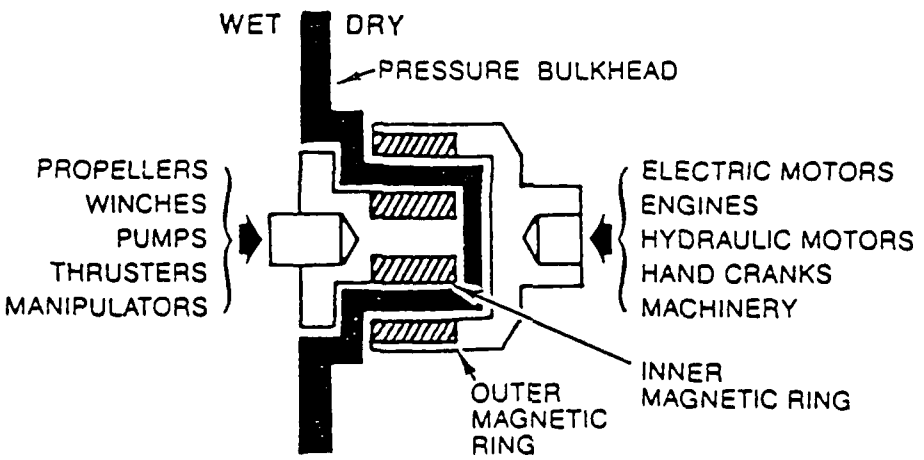

FIGURE 9

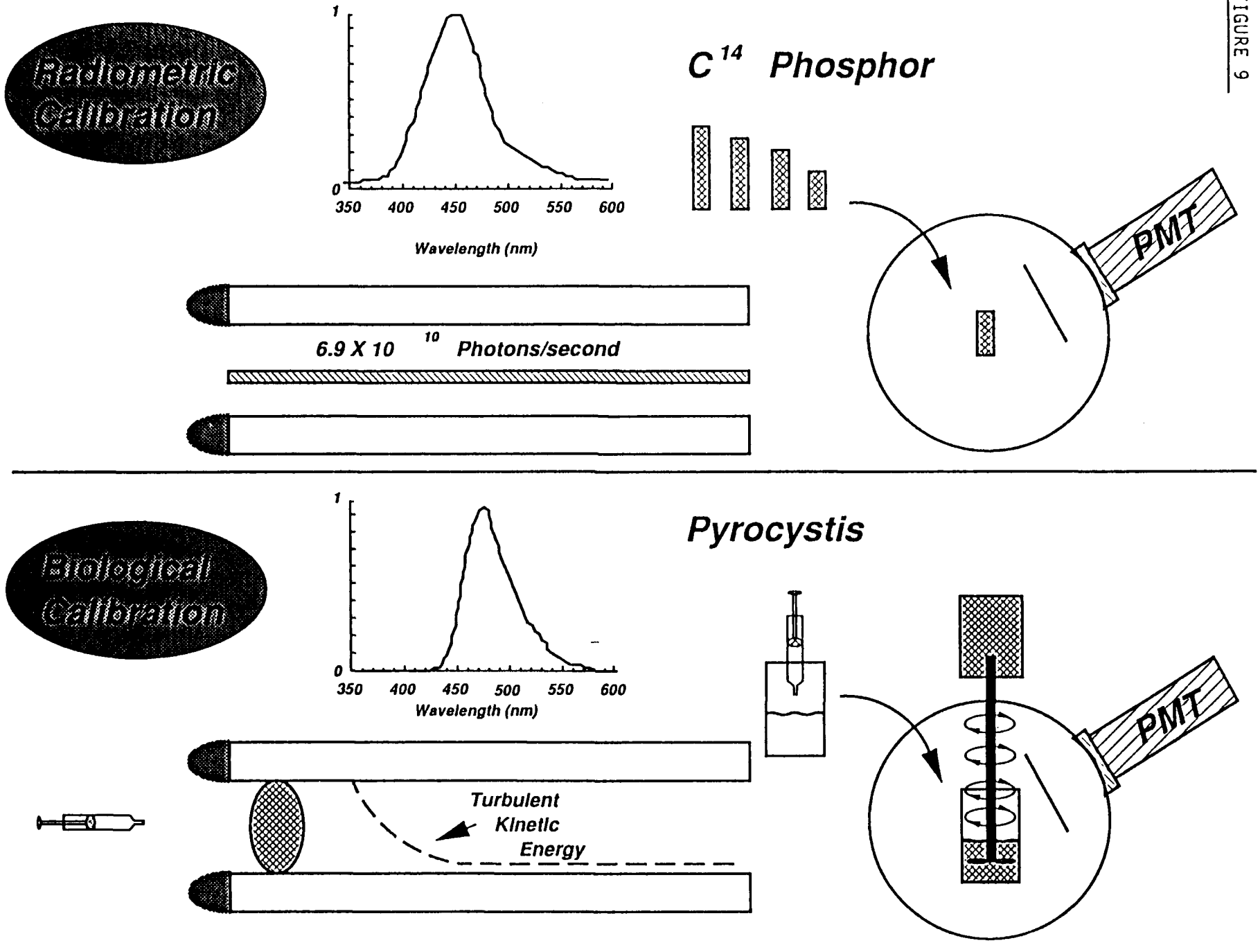
Radiometric Calibration
1
0
350 400 450 500 550 600
Wavelength (nm)
C 14 Phosphor
6.9 X 10 10 Photons/second
PMT
Biological Calibration
1
0
350 400 450 500 550 600
Wavelength (nm)
Pyrocystis
Turbulent
Kinetic
Energy
PMT

FIGURE 10-A

WINCHES—ELECTRIC, PORTABLE

These winches are used to deploy various electronic instruments where size and weight constraints are critical. They are commonly used for water quality monitoring equipment, remote readout current meters, marine photometers, etc. The multi-conductor electrical cable, which is used, is terminated in a low noise, instrumentation grade slip ring assembly. All models are equipped with a manual band brake with positive locking position. A variety of drive mechanisms are available including manual drive, AC or DC from ship's supply, and battery operation.

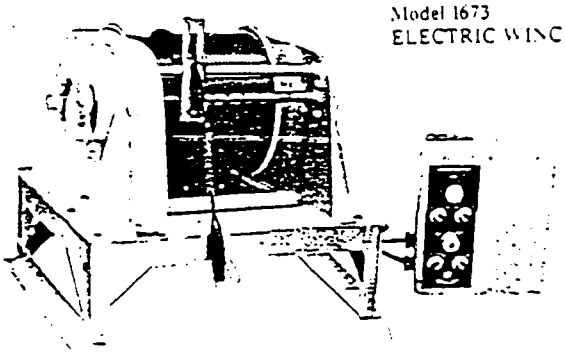

Model 1673
ELECTRIC WINCH

MODEL	710	721-24 721-115	1673-24 1673-115	1673-3 1673-3-LW Level Wind
Capacity (m)	180 m of 12 mm	150m of 11 mm	300m of 11 mm or 500m of 8.5 mm	300m of 11 mm or 500m of 8.5 mm
Load (Kg)	1360	100	100	225
Speed (m/min)	21 m/min	30	30	45
Horse Power	6	3/4	3/4	3
Power In	Hyd 2500 PSI 106 pm	24 VDC 115 VAC	24 VDC 115 VAC	220 AC 1 Ø
Drum Dia. (Cm)	32	18	23	23
Flange Dia. (Cm)	50	39	51	51
Drum Width (Cm)	38	40	46	46
Length (Cm)	115	53	51	110 115
Width (Cm)	69	104	91	91 100
Height (Cm)	62	81	84	91 95
Weight (Kg)	204.5	145 160	105 115	255 295
Slip Rings	14 Channels Standard		Models are available with up to 30 channels of instrument grade slip rings	
Brake	NO	Manual	Manual Electric, fail safe, manual brake	Electric, fail safe, manual brake
Material	Steel	Steel	5086 AL	5086 AL

MODEL 1673

Model 1673 electrical cable winch with electric drive, infinitely variable speed control and electric brake. Capacity of 500 meters of 8.5 mm or 300 meters of 11 mm cable. Standard is operation from 115 VAC (Model 1673-115). Options include operation from 24 volts DC (Model 1673-24); 3 HP drive (Model 1673-3); and an automatic level wind is available for the 3 HP winch (Model 1673-3-LW).

FIGURE 10 B
Cat-22M

OCEANOGRAPHIC COAXIAL CABLE MECHANICAL CHARACTERISTICS

Type	Stock #	Armor OD Inches	Core Dia. – Inches	Inner Armor No./In.	Outer Armor No./In.	Jacket THK./Nt. – Inches	Calc. Armor Ratio	Weight Lbs./1000 Air	Weight Lbs./1000 Sea Water	Break Str. Lbs.	Min. Sheave Dia. (In.)
2-H 160	20160	.160	.078	12/.024	23/.017	–	1.6	45	37	2300	9
2-H-0	20188	.185	.096	18/.018	18/.0245	–	2.3	62	50	2900	10
2-H-251	20251	.251	.147	22/.022	21/.030	–	2.3	104	84	4900	12
2-H-252	20252	.252	.133	18/.0245	18/.035	–	2.3	107	87	5500	14
2-H-255	20255	.255	.147	18/.027	24/.027	–	1.4	107	86	5000	11
2-H-288 J	20288	.244	.190	23/.027	None	025 PE	–	82	53	3000	11
2-H-1	20291	.290	.157	18/.028	18/.0385	–	2.4	145	119	7200	16
2-H-58U	20294	.294	.143	12/.0435	23/.032	–	1.5	146	119	7600	17
2-H-300	20300	.304	.158	18/.032	24/.032	–	1.6	145	116	7400	13
2-H 2	20327	.321	.170	18/.032	18/.0435	–	2.5	176	143	9200	"
2-H-349	20349	.349	.202	18/.037	24/.037	–	1.6	225	187	9500	15
2-H-371	20371	.294	.158	15/.037	24/.031	.028" Ht.	1.5	174	126	10000	15
2-H-59U	20377	.377	.226	18/.0435	30/.032	–	1.4	212	167	10000	"
2-H-4	20431	.434	.232	18/.0435	18/.0575	–	2.5	320	262	16000	23
Triax-6	20470	.295	.161	18/.028	18/.0335	.058 Lead .030 Ny	2.4	497	420	6400	16
2-H-477	20477	.477	.285	18/.054*	30/.042*	–	1.25	354	282	17000	22
2-H-528	20528	.528	.304	18/.056	24/.056	–	1.5	434	346	20000	22
20590	20590	.592	.365	24/.049	24/.063	–	2.0	562	452	24000	25
2-H-213U	20609	.609	.404	22/.059	36/.0435	–	1.06	514	384	26000	24
2-H-679	20679	.669	.417	24/.056	24/.070	–	2.0	680	539	32000	28
2-H-680	20680	.680	.450	22/.065	36/.050	–	1.04	659	514	31000	26
2-H-696	20696	.698	.350	24/.047	24/.059	–	1.05	824	671	45000	27
2-H-725	20725	.725	.470	21/.074	36/.054	–	1.07	764	398	40000	30
Triple Armor					27/.063						
-2 Coax	21148	1.148	.840	36/.070	36/.084	–	1.7	1925	1510	70000	34
Triax	30517	.517	.357	36/.030	–	.050" PE	–	232	139	5500	12
Non-Magnetic Magnetometer Cables – Beryllium Copper Armor											
2-H 161	20161	.157	.089	18/.017	23/.017	–	1.9	46	38	1200	7
RG 58-U	20372	.302	.188	24/.025	24/.032	.035 PE	"	168	120	4000	13

*Stainless Steel
NOTE: All values are nominal

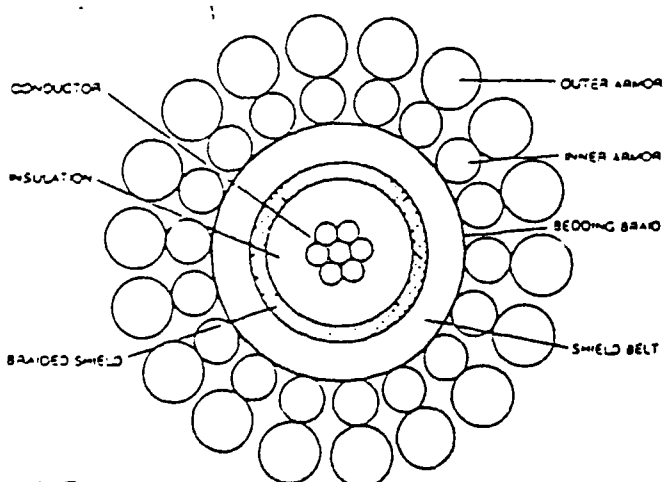

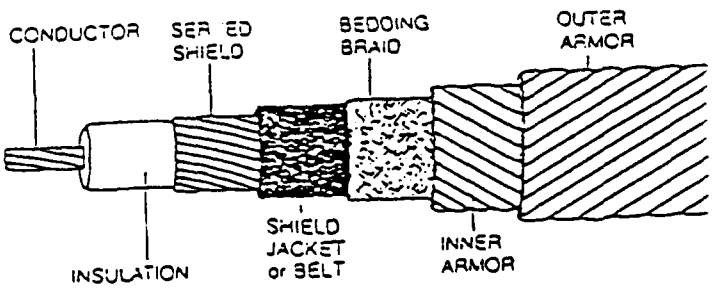

Typical Construction of Armored Coaxial

FIGURE 11

ENGINEERING DATA & SPECIFICATIONS

SPEED SENSOR

TYPE:	Electro-Magnetic, 2 Axis
RANGE:	0-350 cm/sec (0-11.5 ft/sec)
RESOLUTION:	0.2 cm/sec (0.007 ft/sec)
ACCURACY:	2% Reading +/- 1 cm/sec (0.03 ft/sec)

COMPASS

TYPE:	Flux-Gate Magnetometer
TILT:	+/- 25°
RESOLUTION:	0.5°
ACCURACY:	2°

TIME KEEPING

TYPE:	Quartz Oscillator
POWER:	Non-restricted lithium battery
LIFE:	5 years, factory set to GMT (may be reset using a terminal)
ACCURACY:	12 min/year

CONTROL

TYPE:	EPROM Controlled Micro-processor
FORMAT:	Vector average, burst, adaptive, combination; externally programmable and/or default.

POWER SUPPLY

TYPE:	Internal batteries (6 alkaline "D" cells) (Lithium Optional)
ENDURANCE:	2800 hours continuous operation. 5 years total deployment, with on time equal to 2800 hours (Lithium option)

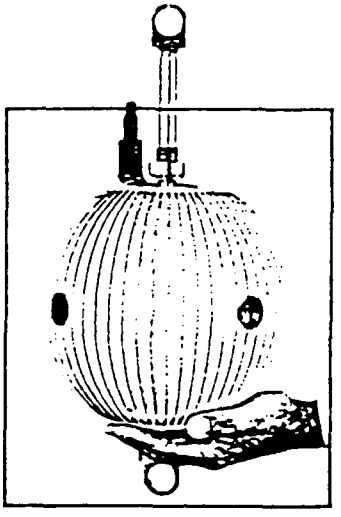

Small and Lightweight.

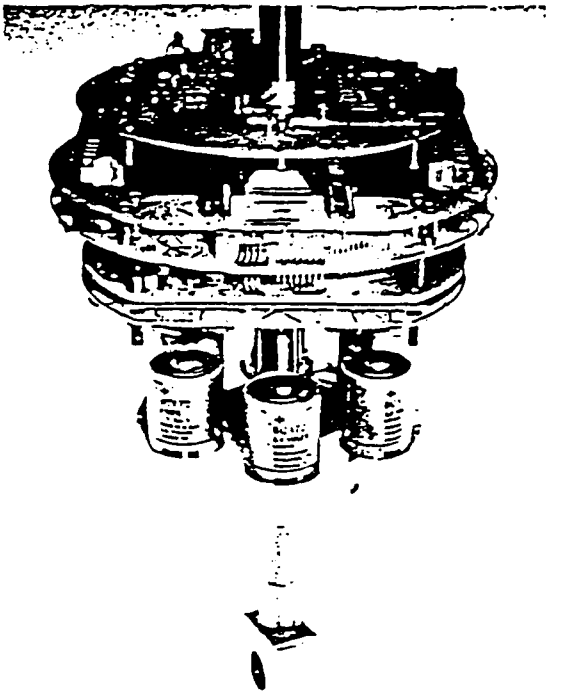

PRESSURE (Optional)

TYPE:	Semi-Conductor Strain Gauge
RANGE:	0-1000 dBar (others optional)
RESOLUTION:	1 dBar
ACCURACY:	5 dBars (Optional, 1 dBar)

TEMPERATURE (Optional)

TYPE:	Thermistor
RANGE:	-2.5 to 36°C
RESOLUTION:	0.05°C
ACCURACY:	+/- 0.1°C
RESPONSE TIME (63%):	1 Minute

CONDUCTIVITY (Optional)

TYPE:	Inductive
RANGE:	1-70 mS/cm
RESOLUTION:	0.1 mS/cm
ACCURACY:	+/- 0.20 mS/cm

MECHANICAL/ENVIRONMENTAL

SIZE:	Sphere, diameter 25 cm (10 inch)
WEIGHT:	Air, 8 kg (24 pounds) Water, 4 pounds
MOORING:	In-line (Optional off-line brackets)
THROUGH LOAD:	4500 kg (10,000 pounds), working
PAD EYES:	Insulating liner, accepts 1.6 cm (⅝ inch) shackle pin
MATERIAL:	Sphere, glass-filled cycloaliphatic epoxy, mooring rod, titanium 6 AL-4V
DRAG:	8 kg (18 pounds) at 250 cm/sec (8 ft/sec)
DEPTH:	1000 meters (3200 ft)
TEMPERATURE:	Storage, -40 to +70°C Operating, -2.5 to +36°C

FIGURE 12

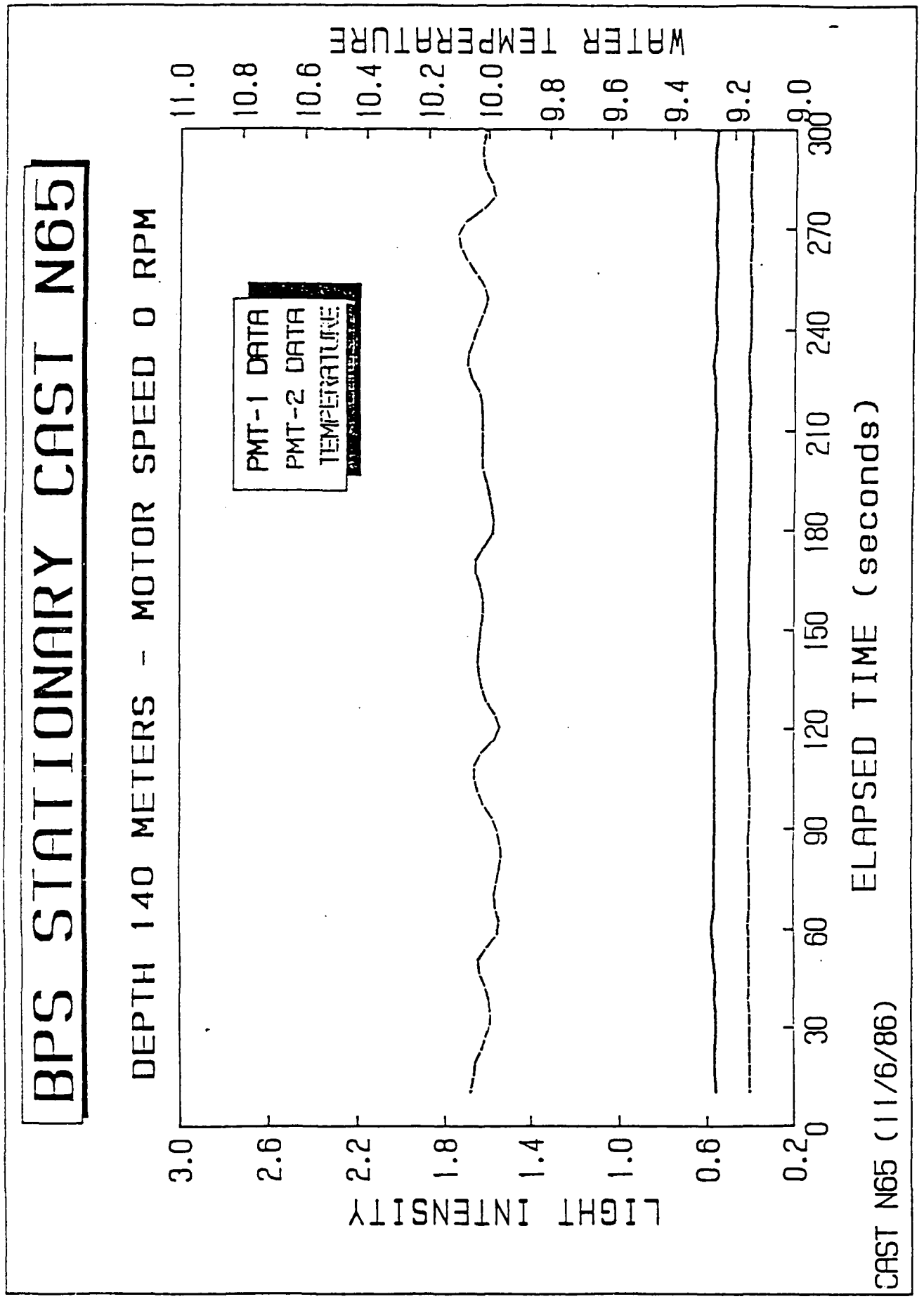
BPS STATIONARY CAST N65
DEPTH 140 METERS - MOTOR SPEED 0 RPM
PMT-1 DATA
PMT-2 DATA
TEMPERATURE
LIGHT INTENSITY
WATER TEMPERATURE
ELAPSED TIME (seconds)
CAST N65 (11/6/86)
3.0
2.6
2.2
1.8
1.4
1.0
0.6
0.2
11.0
10.8
10.6
10.4
10.2
10.0
9.8
9.6
9.4
9.2
9.0
0
30
60
90
120
150
180
210
240
270
300

FIGURE 13

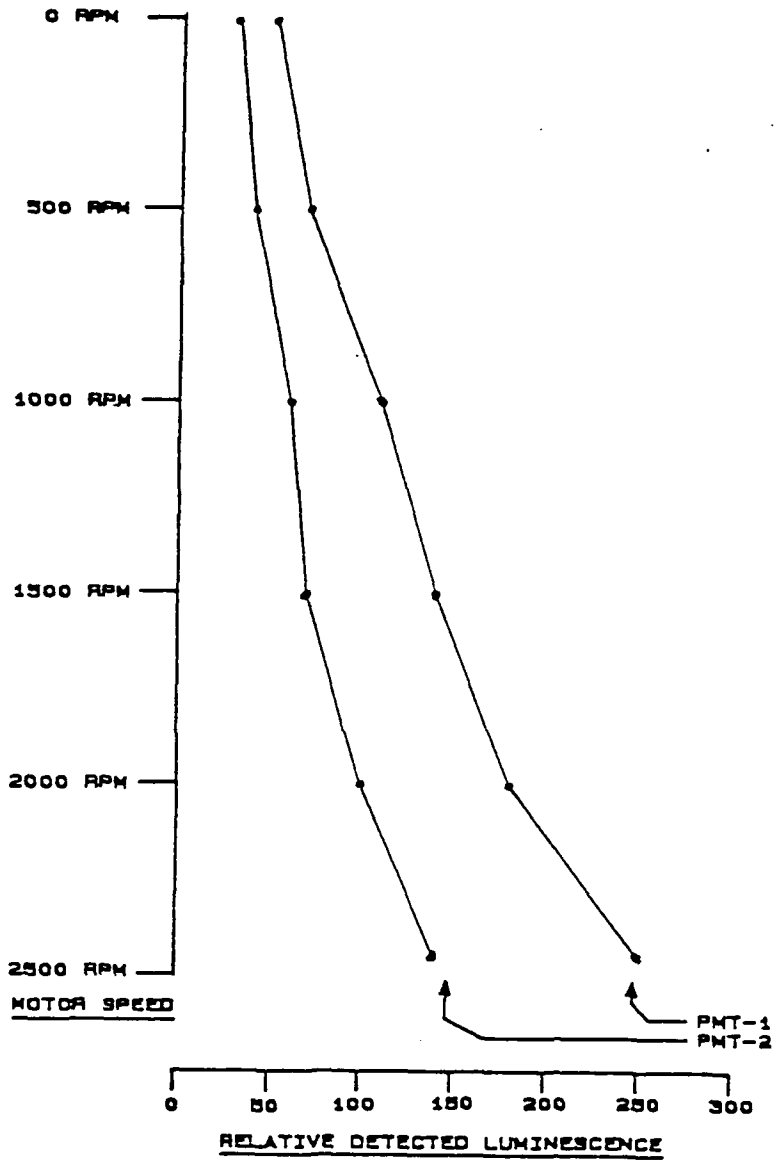

FLOW RATE/BIOLUMINESCENCE PROFILE
CAST NOVEMBER 6, 1986 - DEPTH 60 METERS

FIGURE 14

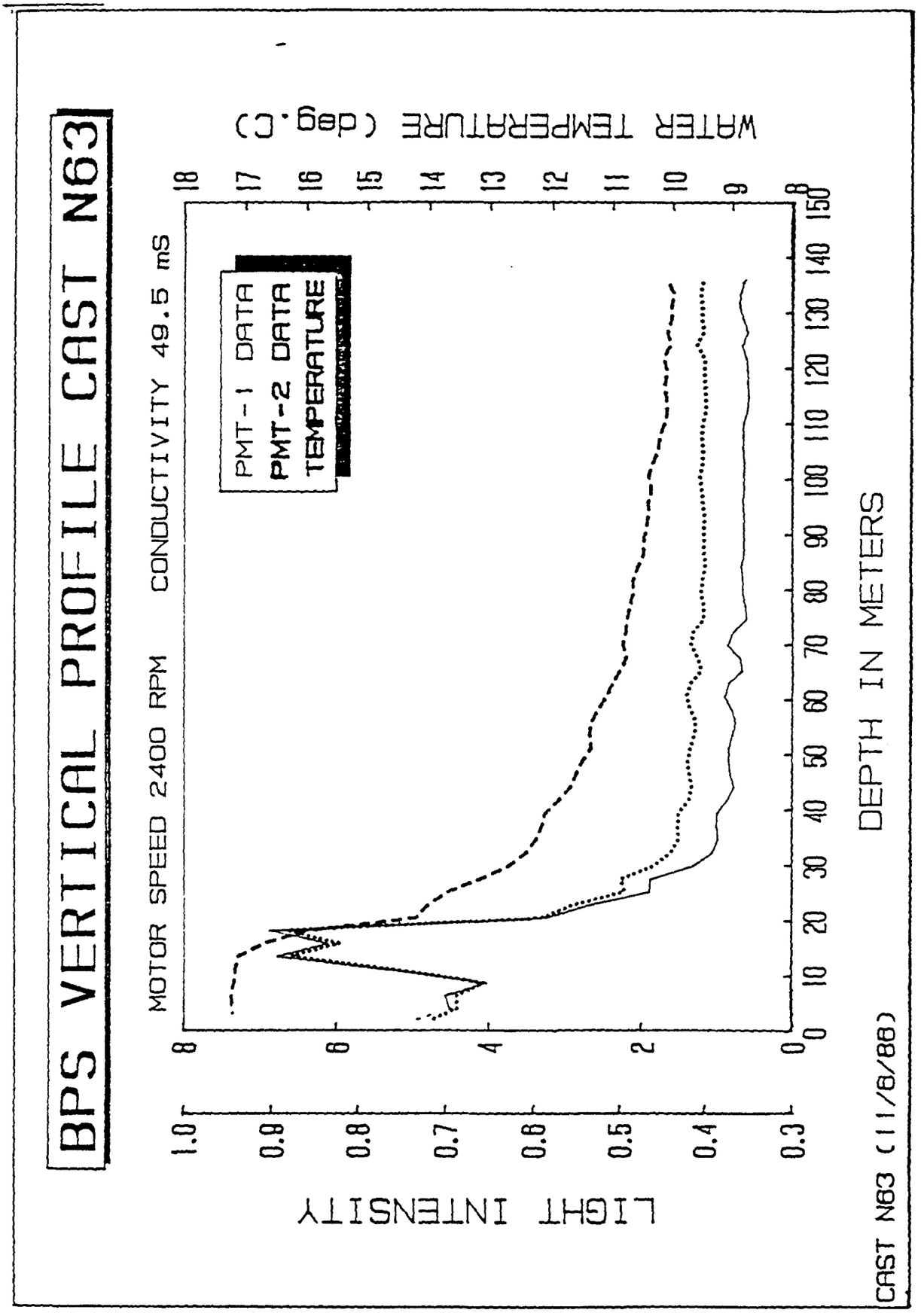
BPS VERTICAL PROFILE CAST N63
MOTOR SPEED 2400 RPM CONDUCTIVITY 49.5 mS
PMT-1 DATA
PMT-2 DATA
TEMPERATURE
LIGHT INTENSITY
WATER TEMPERATURE (deg.C)
DEPTH IN METERS
CAST N63 (11/8/88)

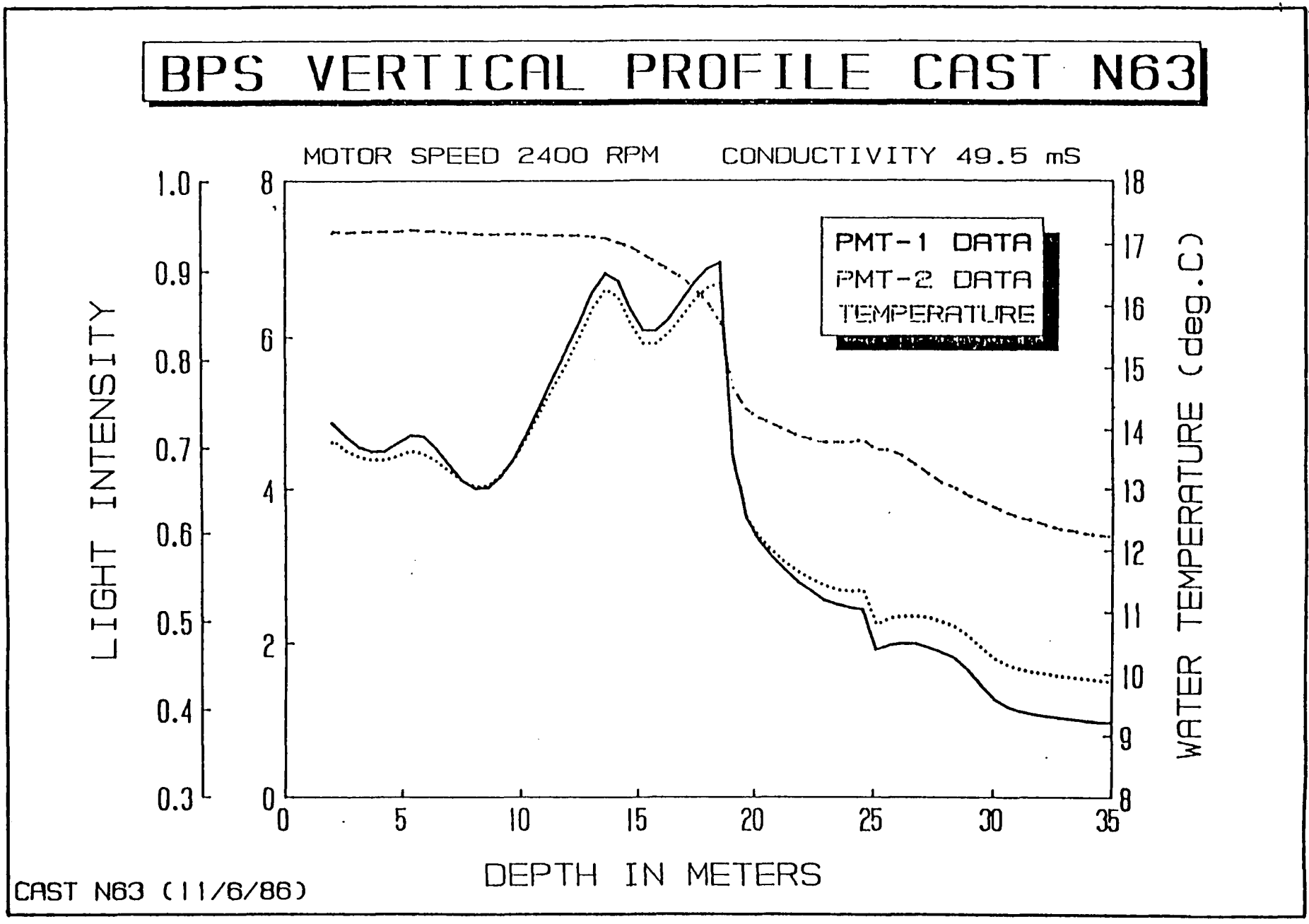
BPS VERTICAL PROFILE CAST N63
MOTOR SPEED 2400 RPM
CONDUCTIVITY 49.5 mS
PMT-1 DATA
PMT-2 DATA
TEMPERATURE
LIGHT INTENSITY
WATER TEMPERATURE (deg.C)
DEPTH IN METERS
1.0
0.9
0.8
0.7
0.6
0.5
0.4
0.3
8
6
4
2
0
18
17
16
15
14
13
12
11
10
9
8
0
5
10
15
20
25
30
35
CAST N63 (11/6/86)

FIGURE 15

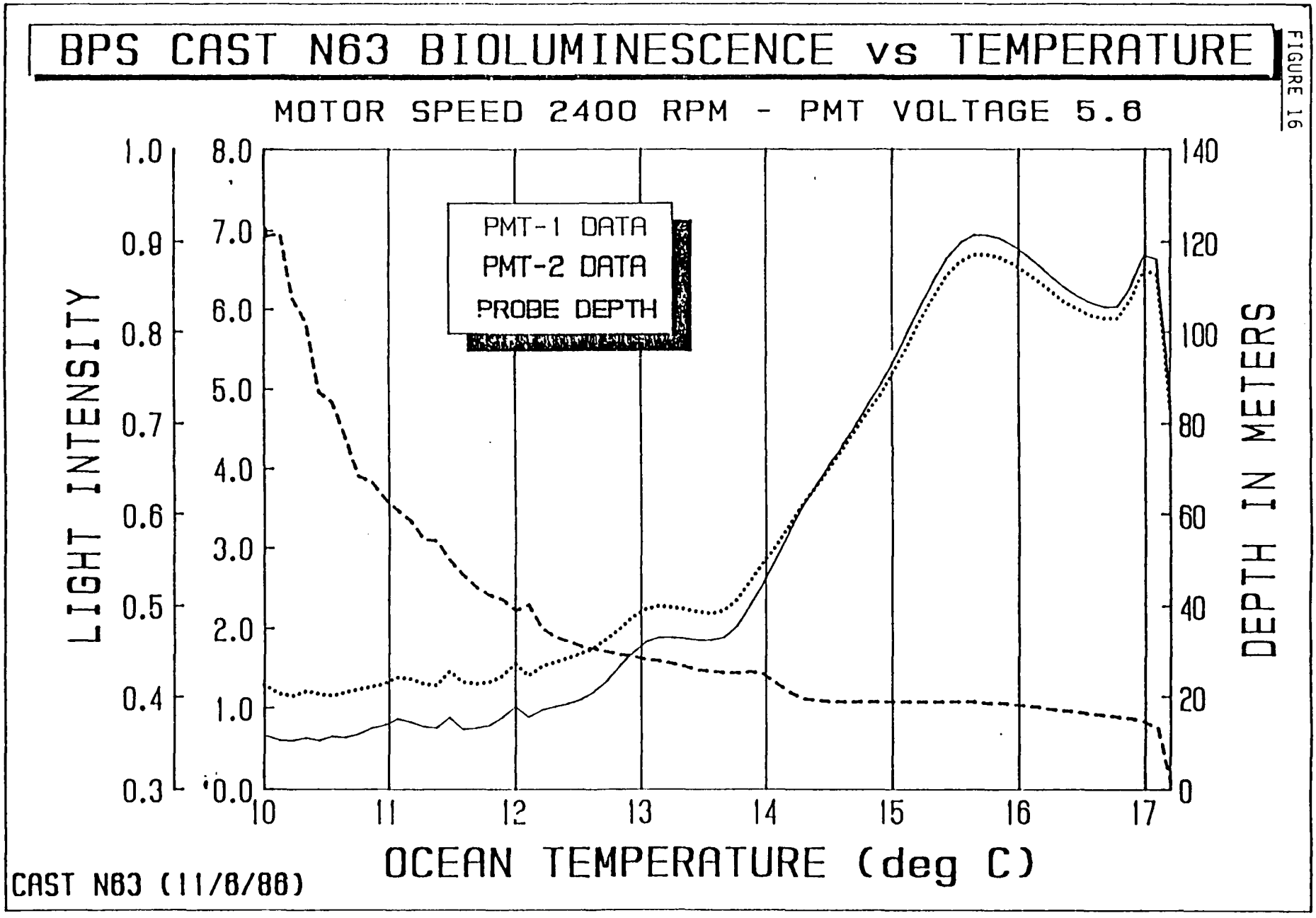
BPS CAST N63 BIOLUMINESCENCE vs TEMPERATURE
MOTOR SPEED 2400 RPM - PMT VOLTAGE 5.6
PMT-1 DATA
PMT-2 DATA
PROBE DEPTH
LIGHT INTENSITY
DEPTH IN METERS
OCEAN TEMPERATURE (deg C)
CAST N63 (11/8/86)
1.0
0.9
0.8
0.7
0.6
0.5
0.4
0.3
8.0
7.0
6.0
5.0
4.0
3.0
2.0
1.0
0.0
140
120
100
80
60
40
20
0
10
11
12
13
14
15
16
17

FIGURE 16

FIGURE 17

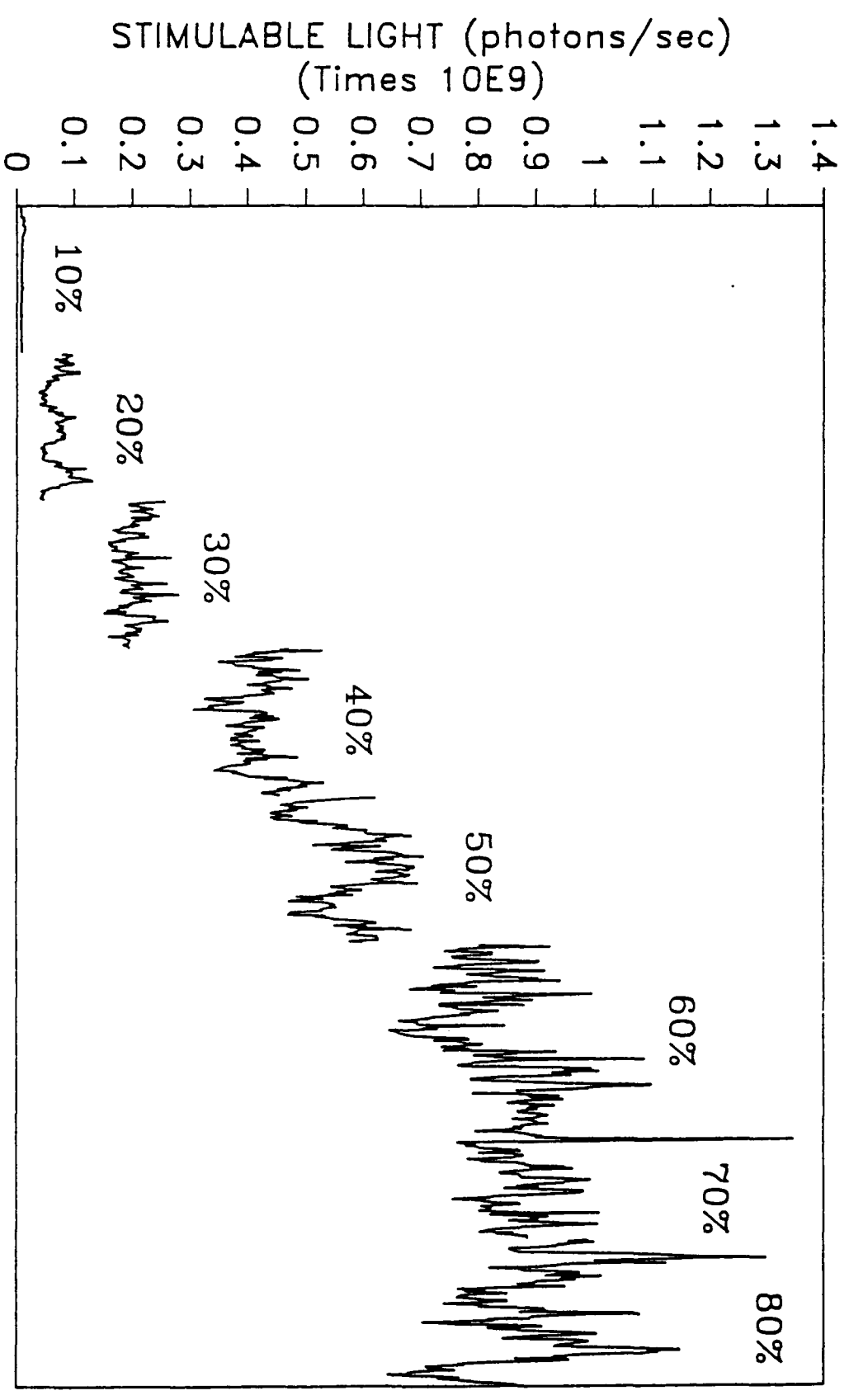

MOTOR SPEED – LIGHT STIMULATION TEST

FIGURE 18

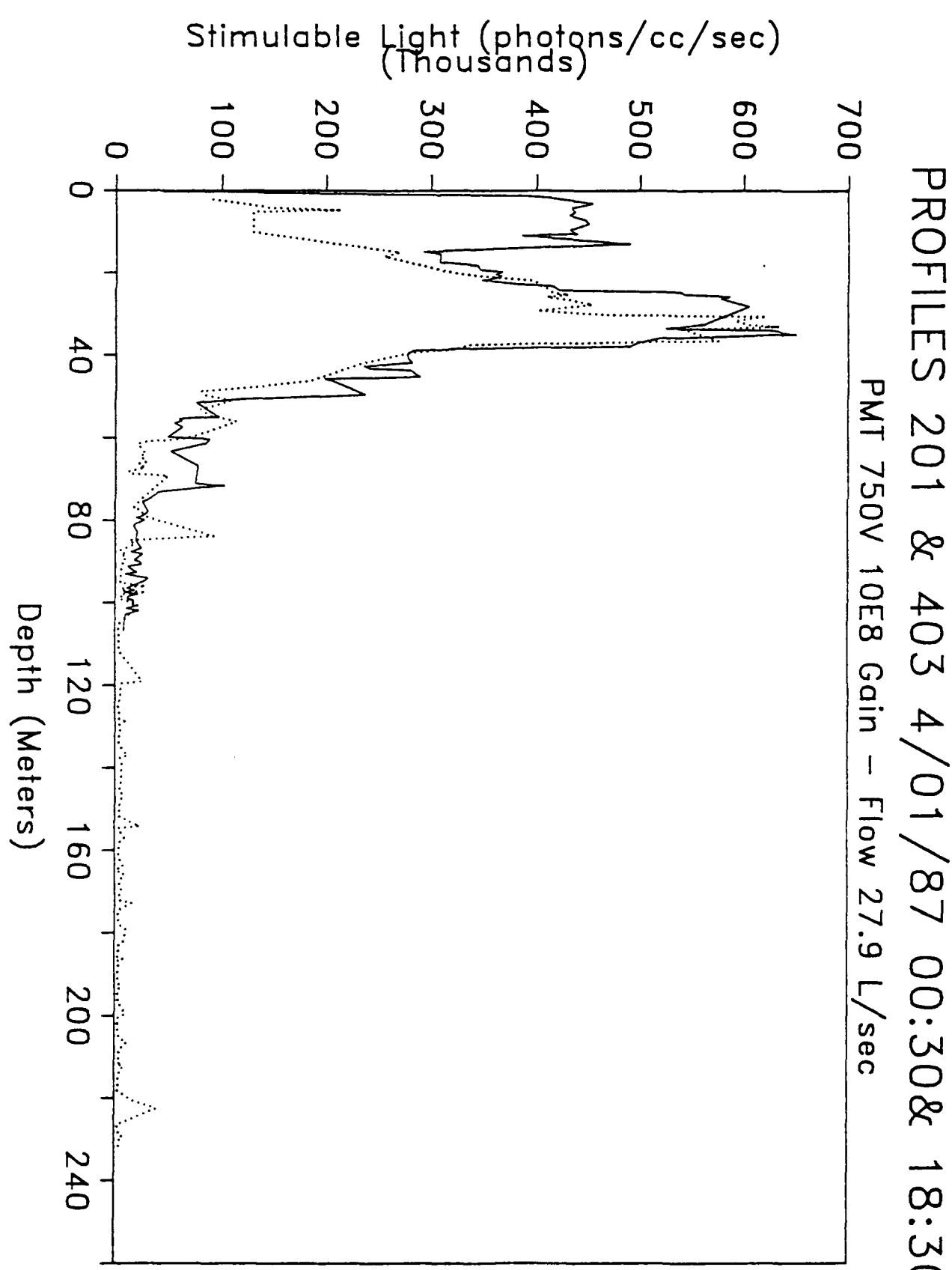
PROFILES 201 & 403 4/01/87 00:30& 18:30
PMT 750V 10E8 Gain – Flow 27.9 L/sec
Stimulable Light (photons/cc/sec)
(Thousands)
0
100
200
300
400
500
600
700
Depth (Meters)
0
40
80
120
160
200
240

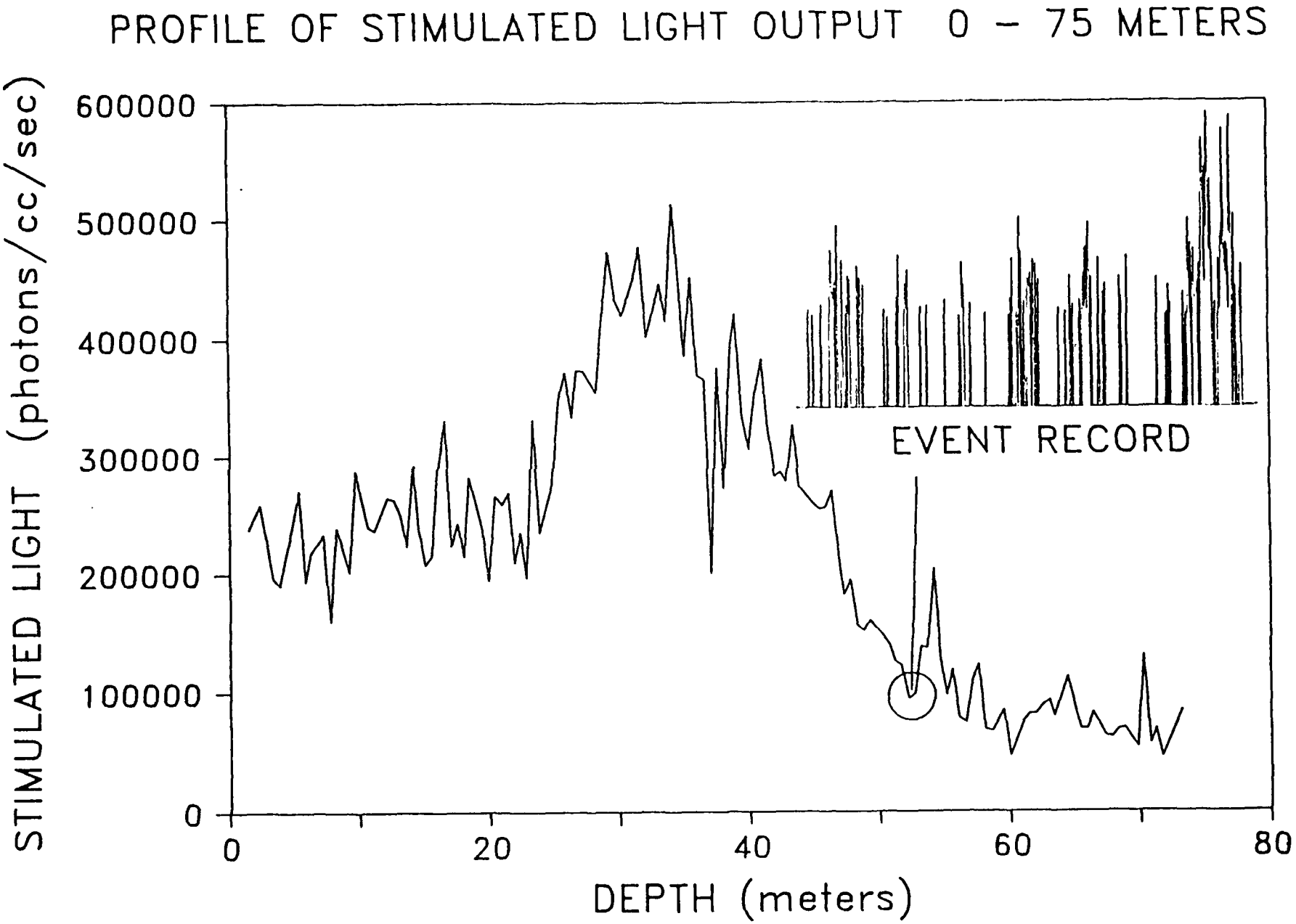
PROFILE OF STIMULATED LIGHT OUTPUT 0 – 75 METERS
STIMULATED LIGHT (photons/cc/sec)
600000
500000
400000
300000
200000
100000
0
0
20
40
60
80
DEPTH (meters)
EVENT RECORD

FIGURE 19

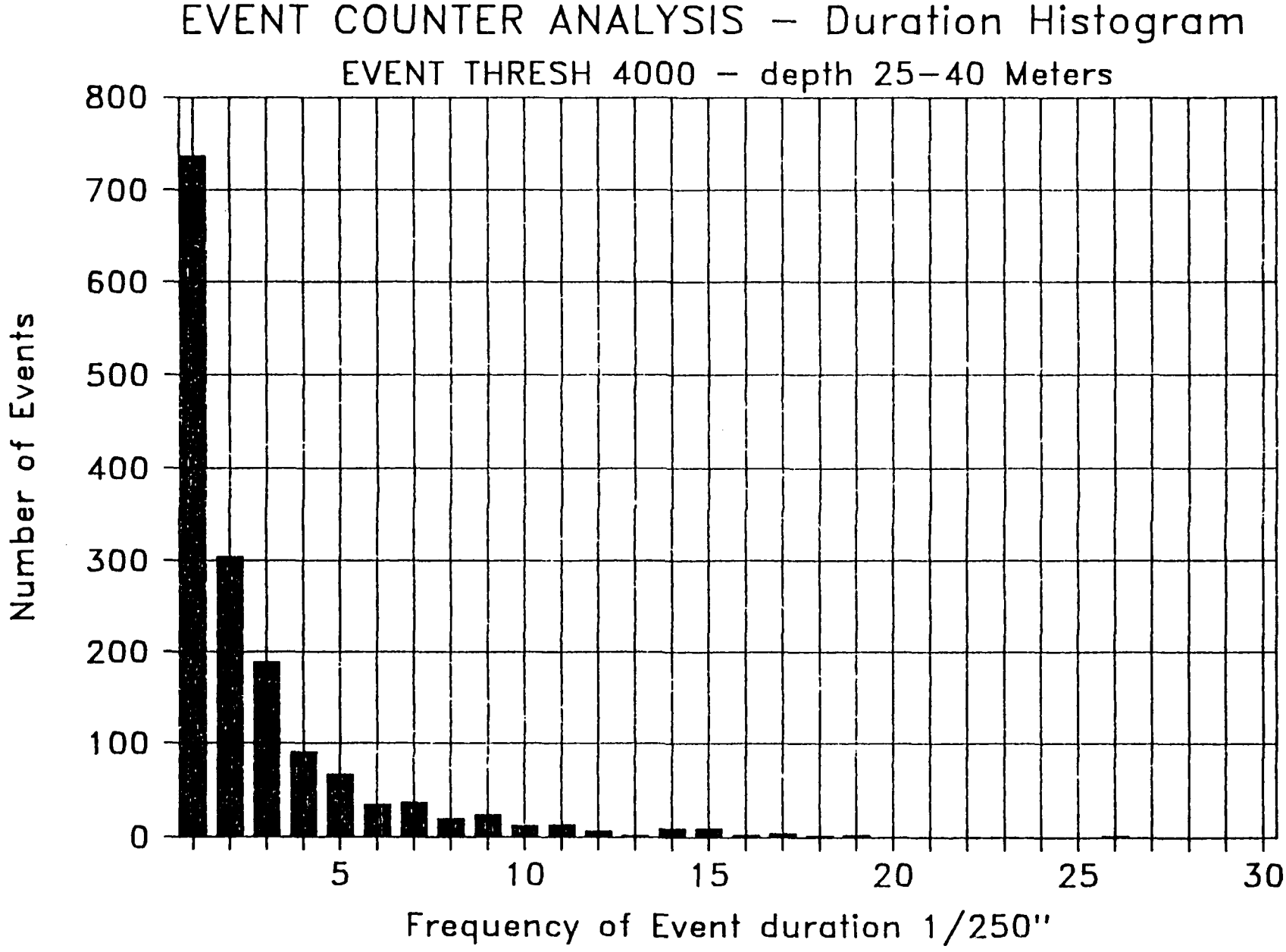
EVENT COUNTER ANALYSIS – Duration Histogram
EVENT THRESH 4000 – depth 25–40 Meters
Number of Events
800
700
600
500
400
300
200
100
0
5
10
15
20
25
30
Frequency of Event duration 1/250"
201.DAT – Depth Profile 3/31/87

FIGURE 20

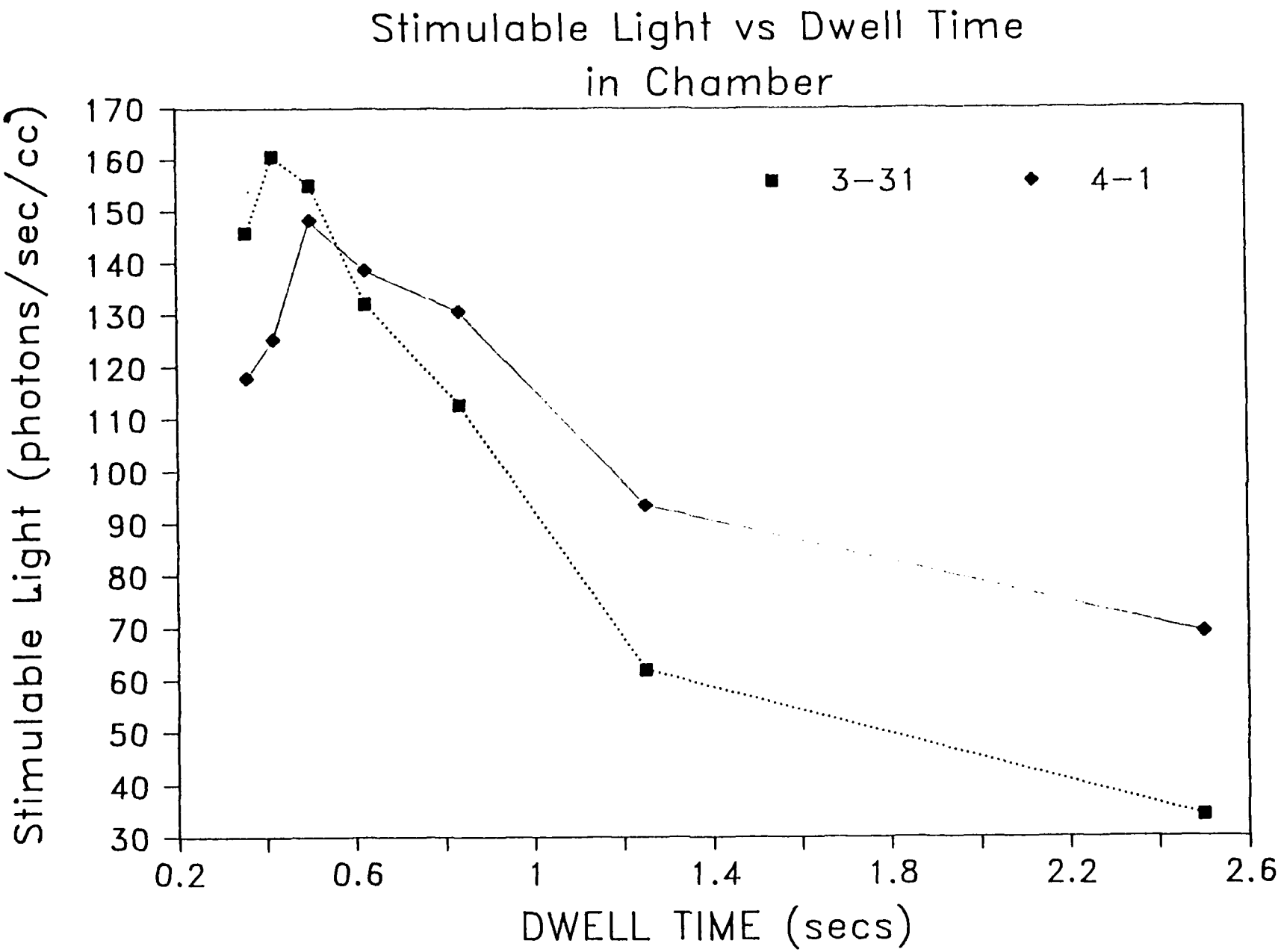
Stimulable Light vs Dwell Time
in Chamber
Stimulable Light (photons/sec/cc)
170
160
150
140
130
120
110
100
90
80
70
60
50
40
30
3-31
4-1
0.2
0.6
1
1.4
1.8
2.2
2.6
DWELL TIME (secs)

FIGURE 21

FIGURE 22

Cruise : NORDA - Sargasso Sea
Date : August 23, 1987
Position : No Navigation
Cast Type : 0-140 Meter Up vs Down Profiles
Cast Duration 7' 30" per cast

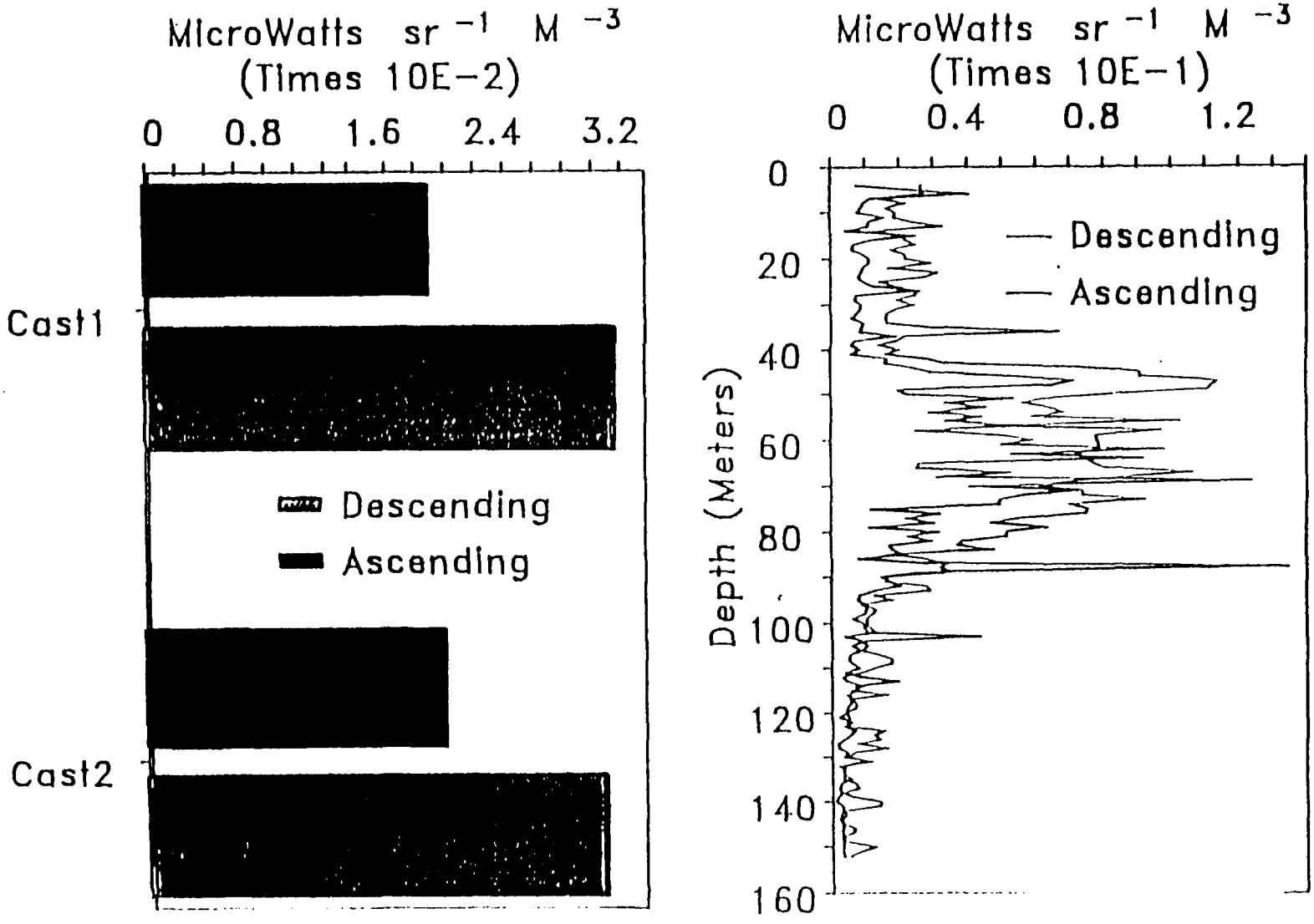

FIGURE 23

Cruise :	NORDA – Sargasso Sea
Date :	August 27, 1987
Position :	LAT 38 10.58 LONG 69 42.66
Cast Type :	0 – 140 Meter Profile
Cast Duration	7 ' 31"

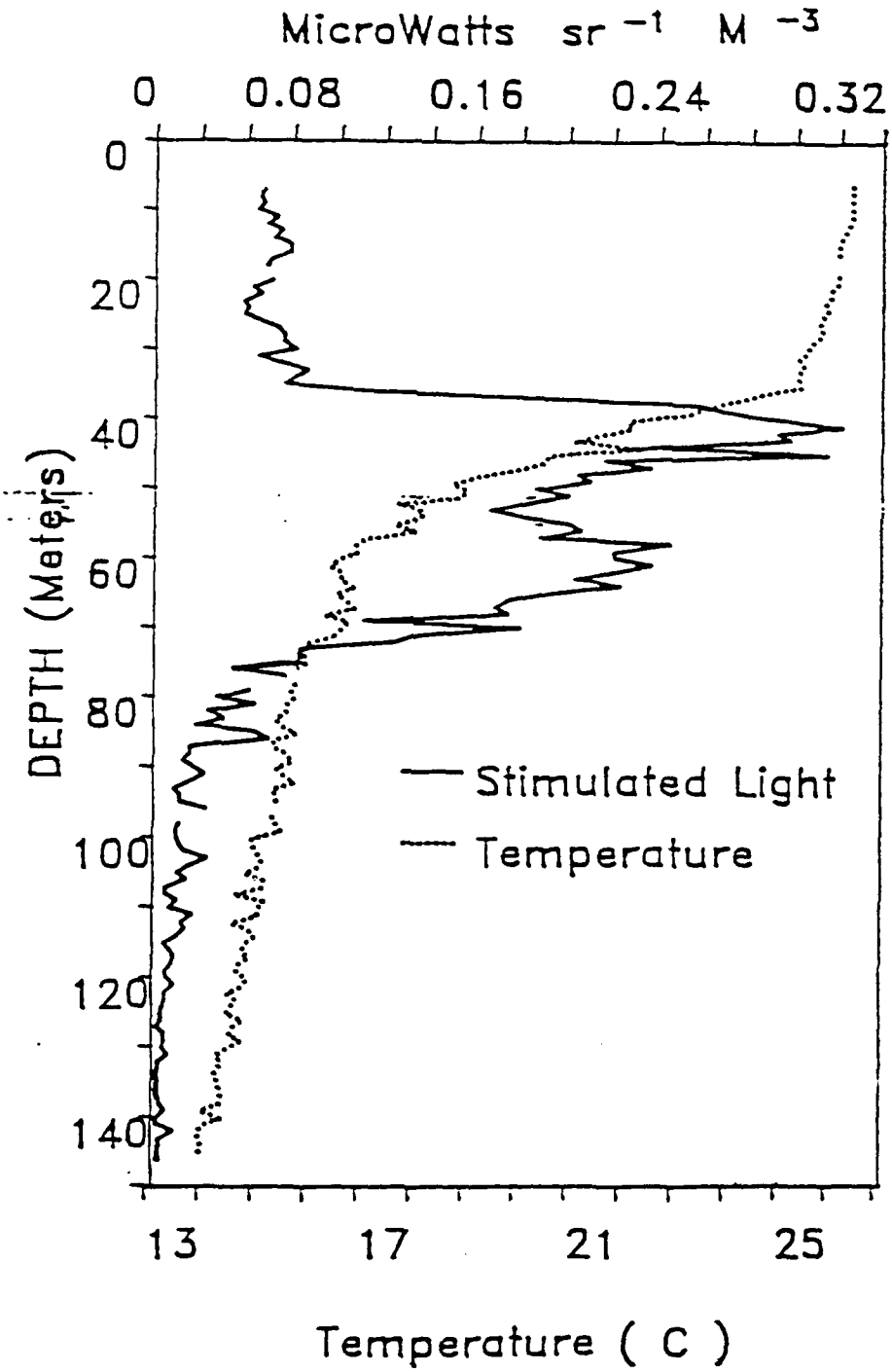

Appendix A

The Bioluminescence Bathyphotometer: Internal Hydrodynamics

Sally MacIntyre
Assistant Research Engineer
Marine Science Institute
University of California
Santa Barbara, California 93106

The bioluminescence bathyphotometer is a device to trigger bioluminescence in organisms. The exact cause of mechanically induced bioluminescence is uncertain: it may be shear, pressure fluctuation, stretching or twisting of the organism's outer membrane in the case of unicellular organisms, or similar effects on mechanosensory receptors of metazoans. Associated with turbulent flows are vorticity, shear, pressure and velocity fluctuations, any one of which is likely to cause bioluminescence. One approach for stimulating bioluminescence is to generate a turbulent flow within the bathyphotometer. Because of its high pumping rates and large diameter, Reynolds numbers in the bathyphotometer are higher than 120,000 and the flow is turbulent. The bathyphotometer, however, is broad in comparison to its length; the flow inside it will never become fully developed. In consequence, the turbulent intensity within the core of the flow is likely to be quite low. A distance of 25 to 40 diameters would be required for the turbulence generated at the walls to spread across the device. In fact, at the entrance to the test section where bioluminescence will be measured, the computed boundary layer thickness is only 1 cm (Fox and McDonald 1973). To generate turbulence in the central portion of the bathyphotometer the flow must be perturbed. Classically perturbations have been made with grids comprised of round or square bars (Batchelor 1953) and a solidity less than 34% (Corrsin 1966). Homogeneous turbulence occurs downstream of the grid. An alternate way to generate a turbulent core is with a helical vane whose development is long enough so that the turbulent boundary layer on each blade becomes thick enough to coalesce with that of its neighbor.

We ran a series of experiments to determine the flow fields within the bathyphotometer when there was no device to perturb the flow, with two

grids with different size openings, and with a free spinning helical vane. We measured instantaneous velocities with a laser-Doppler velocimeter at three positions within the test section and computed mean velocities, turbulent velocities, and the turbulent kinetic energy of the flow. The data will assist in the selection of the appropriate stimulus for bioluminescence as well as to calibrate the bathyphotometer.

Flow speeds were measured with a laser-Doppler velocimeter (LDV) and counter processor in forward scatter mode (Disa Electronics 5 mw helium-neon laser). The beam was transmitted through 1/8" optical flats ground into the bathyphotometer to which were glued 1/8" thick plexiglas. The grids were fabricated with plexiglas into which square bars were milled. The larger of the two grids had bars 0.48 cm in width, a distance of 2.54 cm between centers, and a solidity of 31.9%. The smaller grid had bars 0.31 cm in width, a distance between centers of 1.55 cm, and a solidity of 32%. The vane was six-bladed, 8 cm in length, and had a pitch of 45 cm. The vane also serves as a light baffle and flowmeter and is expected to experience less clogging by organisms. The bathyphotometer was positioned for testing near the rear of a 70 ft. long tilting flume 3 ft. deep and 3 ft. wide. The tilting flume was partitioned to create a dry well around the mid-section of the bathyphotometer where LDV measurements could be made. Velocity transects radially across the bathyphotometer were made at 3 positions chosen to give a reasonable range of the ratio of the distance downstream from the grid to the mesh length of the grids. The location of the measurement volume of the LDV inside the bathyphotometer was measured relative to the outer wall of the bathyphotometer and was corrected for transmittance through materials with different refractive indices as in Durst, Melling, and Whitelaw (1976, p. 18). The refractive

index used for plexiglas was 1.5. Because of the change in beam angle due to different refractive indices and because of increased reflections by the laser beams near the walls, profiles span only three quarters of the channel.

Results

Velocity profiles at position 3 with and without the two grids are presented in Fig. 1. The motor was running at 100% of its capacity. With a clear channel, the velocity profile was blunt and flow speeds were ca. 3.9 $m \cdot s^{-1}$ in the center of the channel. Profiles were also blunt with the grids in place but velocities were reduced. With the 0.5 inch grid, velocities were highest ca. 2 cm from the walls, an effect also observed at position 4. Turbulent intensity is the rms velocity, $\overline{u^2}^{1/2}$, divided by the mean velocity where u is the fluctuation from the mean velocity. Turbulent intensities in the central portion of the channel are highest with the larger grid in place and are more uniform across the channel with the grids than without (Fig. 2). The ratio $\overline{u}^2/\overline{U}^2$ is the ratio of the turbulent kinetic energy of the flow to the mean kinetic energy of the flow. This ratio is plotted against distance downstream normalized by the mesh length of the grids (Fig. 3). The data had a power low fit as did that of Warhaft and Lumley (1978).

Velocity profiles with the vane in place are not uniform across the channel (Fig. 4). The mesh length for the vane was taken as the separation between the blades at the radial position that bisects the cross-sectional area of the helical vane. Again the relation of TKE/KE to normalized distance downstream was curvilinear (Fig. 5).

The average ratio of TKE/KE from 3 or 4 vertical positions for the two grids and the vane are plotted against distance downstream from the grid in Fig. 6. TKE was comparable for the vane and the larger grid at the three positions whereas TKE for the smaller grid was considerably less. Without a grid, TKE/KE was extremely low. TKE decreased from position 3 to position 5, 40 cm downstream.

Noise levels were too high near the wall to obtain a good velocity profile within the boundary layer to determine if velocities scale with the logarithm of distance from the wall. If this assumption is met, shear stress (τ) can be computed from velocities measured within the boundary layer. Boundary layer thickness is $\delta = 0.376 \times \left(\frac{U_\infty x}{\nu}\right)^{-\frac{1}{5}}$ where U_∞ is velocity in the free stream away from the wall, x is distance from the entrance, and ν is kinematic viscosity. The equation for shear stress is $\tau = \rho u_*^2$ where u_* is computed from $U_z/u_* = (1/\kappa)(\ln(zu_*/\nu))+5.5$ (Schlicting 1968) where u_* is the friction velocity, κ is von Karman's constant, and z is depth. At position 4, the boundary layer thickness was computed to be 1.3 cm; we were able to make measurements 1.4 cm from the wall. Assuming these measurements were within the boundary layer, the shear stress at the wall was 36 dynes$\cdot$cm^{-2}. Assuming the law of the wall relation and the boundary layer scaling apply when the small grid is in place, shear stresses at the wall ranged from 55-90 dynes$\cdot$cm^{-2}. The shear stress generated at the wall diffuses throughout the channel reaching a value of zero at the center.

The Reynolds stresses in the core of the flow should be of the same order of magnitude or less than the wall shear stress, and Batchelor (1953,

p. 110) states that they are proportional to 0.5 $\overline{u_1^2}$ where u_1 is axial velocity. In other words, the Reynolds stresses are proportional to the turbulent kinetic energy. Values of 0.5 $\overline{u_1^2}$ were highly variable when the channel was clear probably because of measurement problems. Values of kurtosis were larger than three and the data were highly skewed. In the core region, however, when kurtosis was less than 10, 0.5 $\overline{u_1^2}$ averaged 66 $cm^2 \cdot s^{-2}$ at position 3 and 13 $cm^2 \cdot s^{-2}$ at position 4; these values are comparable to or less than the wall shear stresses and may well approximate the Reynolds stresses.

Incorporating a grid or vane into the flow increases the stresses in the flow. At position 3 with the large grid in place, 0.5 $\overline{u_1^2}$ ranged from 338 to 462 $cm^2 \cdot s^{-2}$; with the small grid it ranged from 184 to 242 $cm^2 \cdot s^{-2}$; and with the vane it ranged from 328 to 490 $cm^2 \cdot s^{-2}$. At position 4, 0.5 $\overline{u_1^2}$ ranged from 181 to 192 $cm^2 \cdot s^{-2}$ for the large grid; from 91 to 119 $cm^2 \cdot s^{-2}$ for the small grid, and from 196 to 214 $cm^2 \cdot s^{-2}$ for the vane. For these measurements values of kurtosis were near 3 and skewness ranged from -0.5 to 0.7. The grids and vane initially increase the stress in the flow over that generated near the wall; the added stress decays downstream.

The effect of the turbulent kinetic energy on organisms in the flow depends on the size of the eddies in the flow and the energy associated with these eddies. Previous experiments have shown a peak in the energy spectrum behind grids at a wavelength corresponding to the mesh length of the grid. This energy is transferred to smaller eddies, but the rate at which the energy is transferred determines the amount available at smaller wavelengths. Knowing the quantity of energy available at wavelengths comparable in size or slightly larger than the organisms in the flow would

require measurements of the energy spectrum. Energy spectra are calculated from time series of velocity measurements obtained with hot film anemometry or laser-Doppler velocimetry. Because we used a counter processor to process the LDV signal, our data were not obtained at even time intervals. Without equally spaced data, spectral analysis is an extremely difficult problem.

Motor speed and core velocities show a linear relation, and turbulent intensity is independent of motor speed (Figs. 7 and 8). At position 5, Reynolds stresses, again approximated by the relation $0.5\ \overline{u_1^2}$, averaged 102 $cm^2 \cdot s^{-2}$ at 100% of the motor speed, 43 $cm^2 \cdot s^{-2}$ at 80% of the motor speed, 41 $cm^2 \cdot s^{-2}$ at 60% of the motor speed, and 15 $cm^2 \cdot s^{-2}$ at 40% of the motor speed (Fig. 9).

Discussion

Adding a vane or a grid to the interior of the bathyphotometer clearly increases the turbulent kinetic energy and associated Reynolds stresses in the core region of the flow downstream of the vane or grid. In addition, a range of stresses can be generated by varying the motor speed. The relation of TKE/KE to normalized distance downstream is independent of the mesh length of the grid and suggests that the initial increase in TKE supplied to the flow is comparable for the two grids. Because of the difficulty in normalizing the downstream distance for the helical vane, assessing the increase in TKE behind it is impossible. Downstream its influence on the flow is comparable to that of the larger grid. TKE is at smaller wavelengths and decays more rapidly downstream of the smaller grid, features which make the small grid the most appropriate to use. It provides an intense initial stimulus with a rapid decay downstream. Light

baffling will probably be necessary and the helical vane will be required. Because the helical vane complicates the flow in the core region of the bathyphotometer, the stimulation organisms will receive will be highly dependent upon their position in the flow. To calibrate the flow field with it in place will require velocity measurements in the radial and axial directions.

References

Batchelor, G.K. 1953. The Theory of Homogeneous Turbulence. Cambridge University Press.

Corrsin, S. 1963. Turbulence: experimental methods. In S. Flugge and C. Truesdell, eds. Encyclopedia of Physics, vol. 8(2). Fluid Dynamics II. Springer-Verlag, Berlin. pp. 524-590.

Durst, F., A. Melling, and J.H. Whitelaw. 1976. Principles and practice of laser-Doppler anemometry. Academic Press.

Fox, R.W. and A.T. McDonald. 1973. Introduction to Fluid Mechanics. John Wiley and Sons, NY.

Schlichting, H. 1968. Boundary-Layer Theory. McGraw Hill, NY.

Warhaft, Z., and J.L. Lumley. 1978. An experimental study of the decay of temperature fluctuations in grid-generated turbulence. J. Fluid. Mech. 88: 659-684.

velocity vs. radial position

position 3

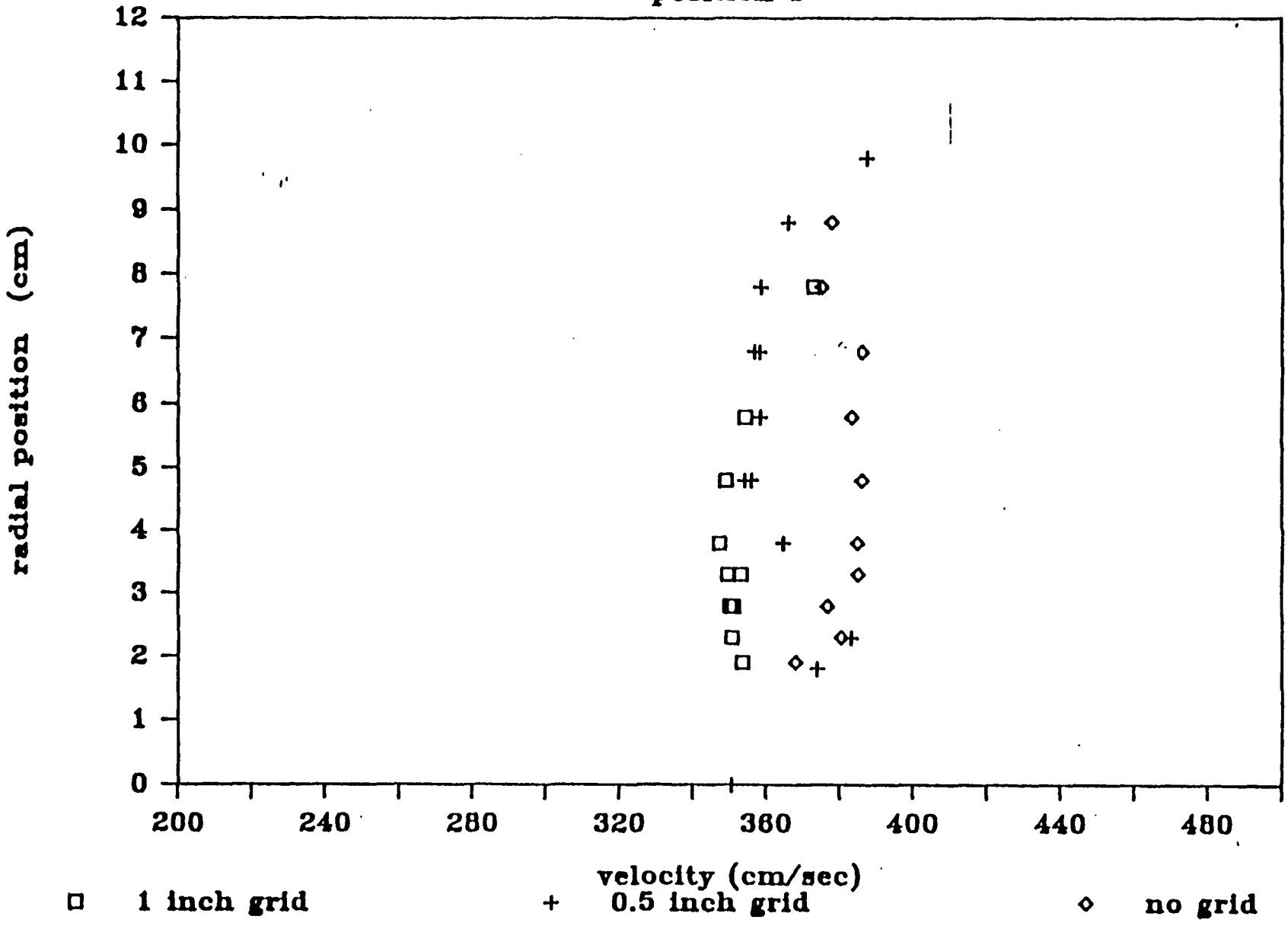

turbulent intensity vs. radial position

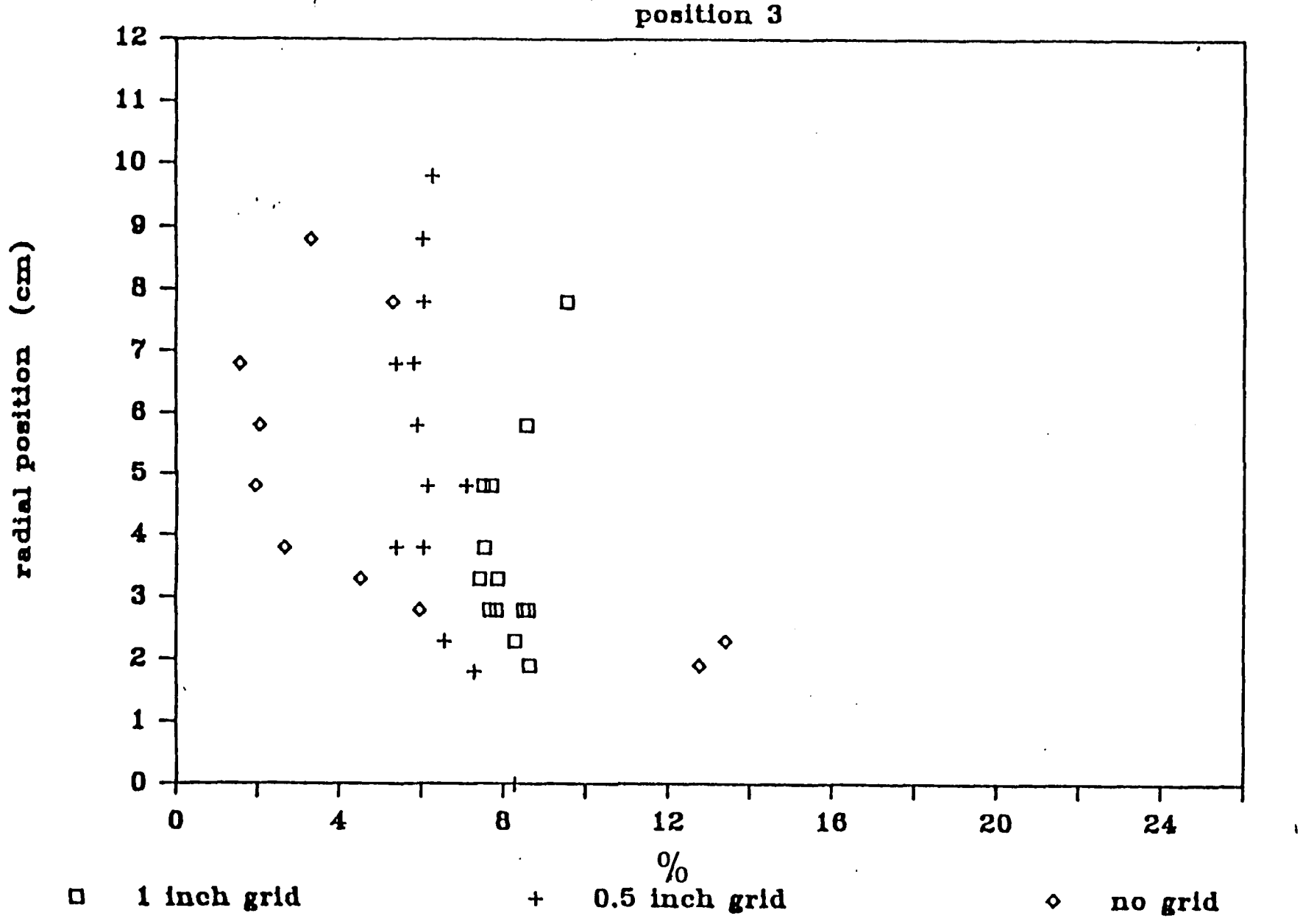

tke/ke *1000 vs normalized distance

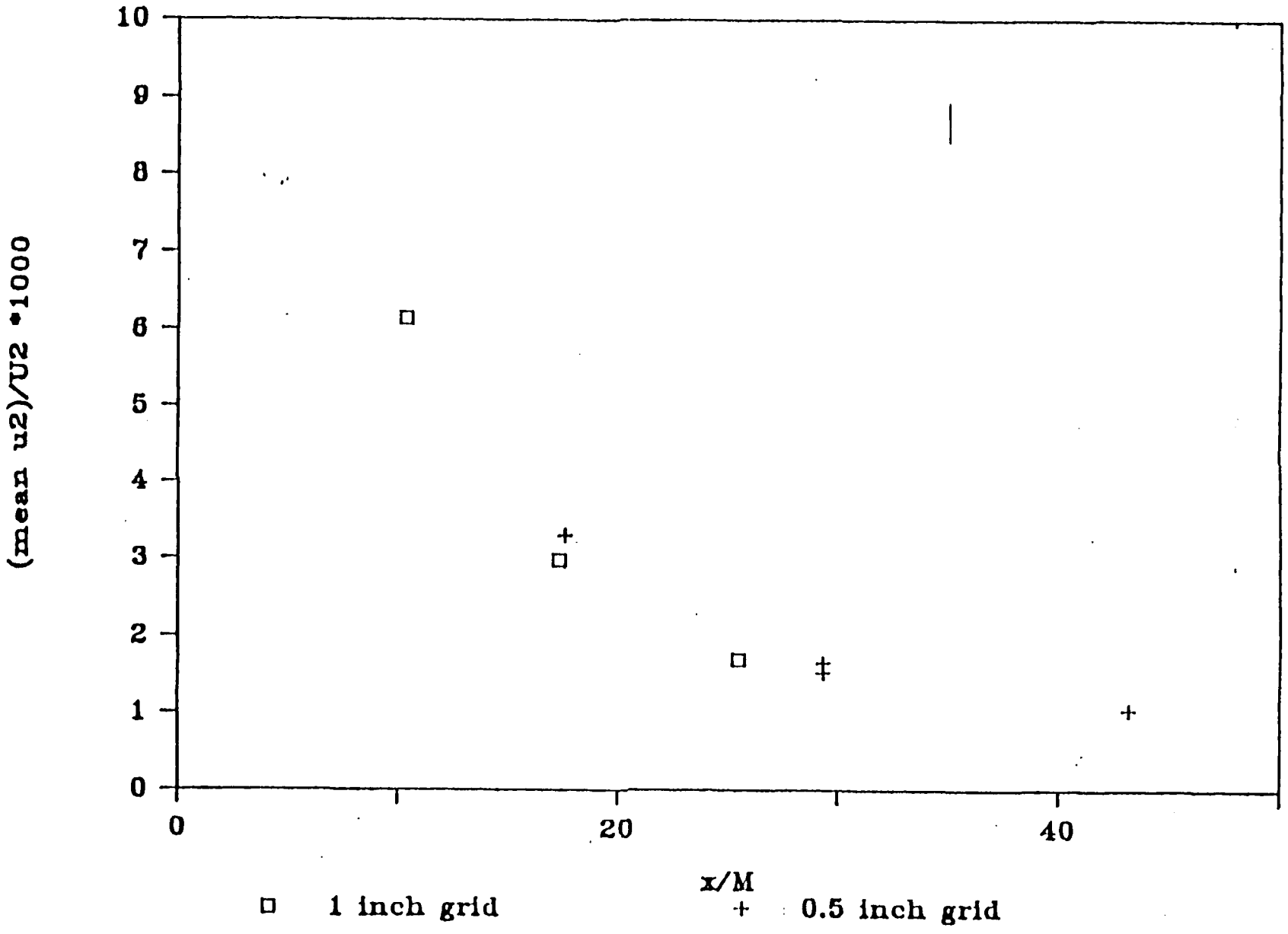

velocities at positions 3,4, and 5

vane in place

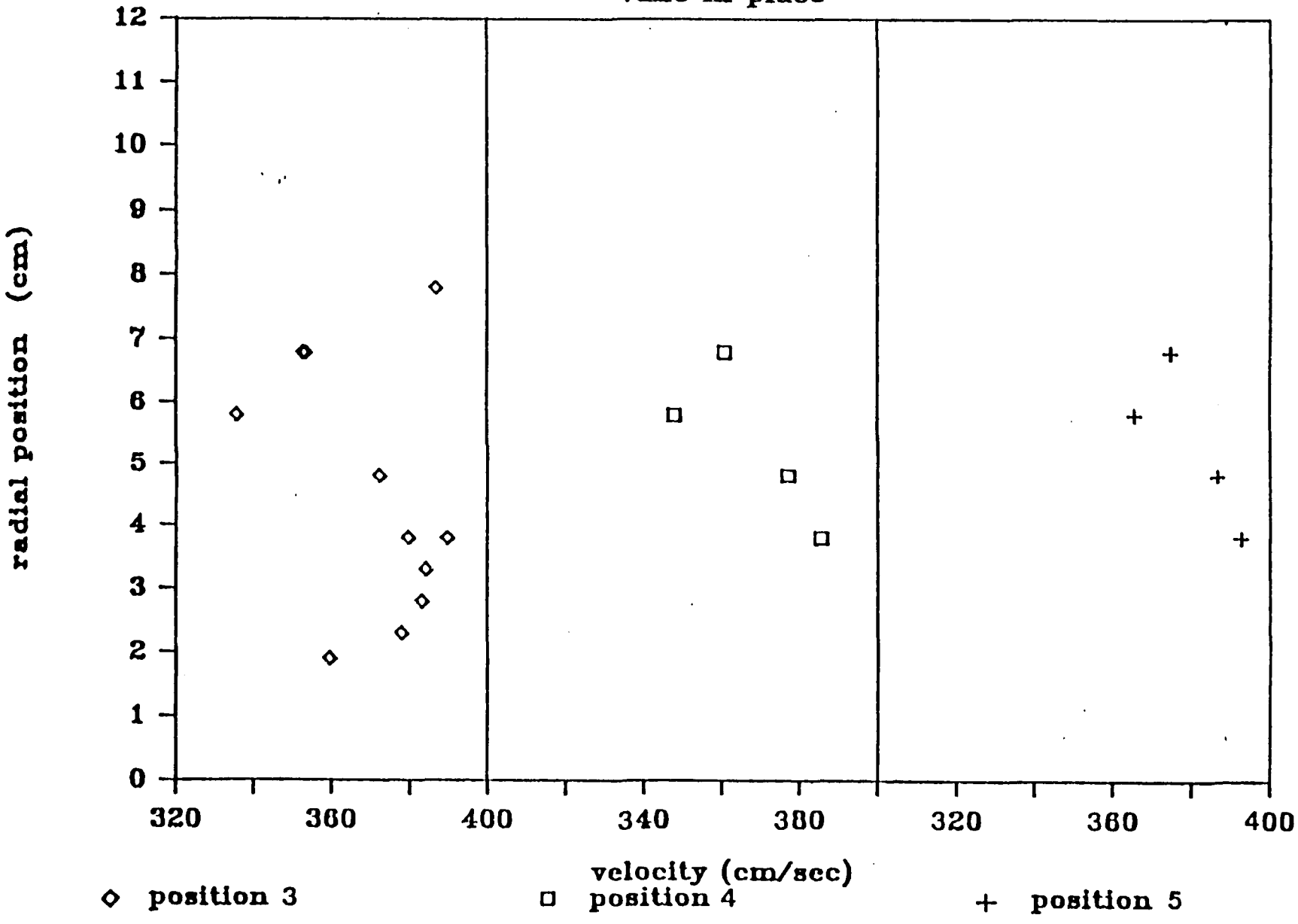

tke/ke *1000 vs distance

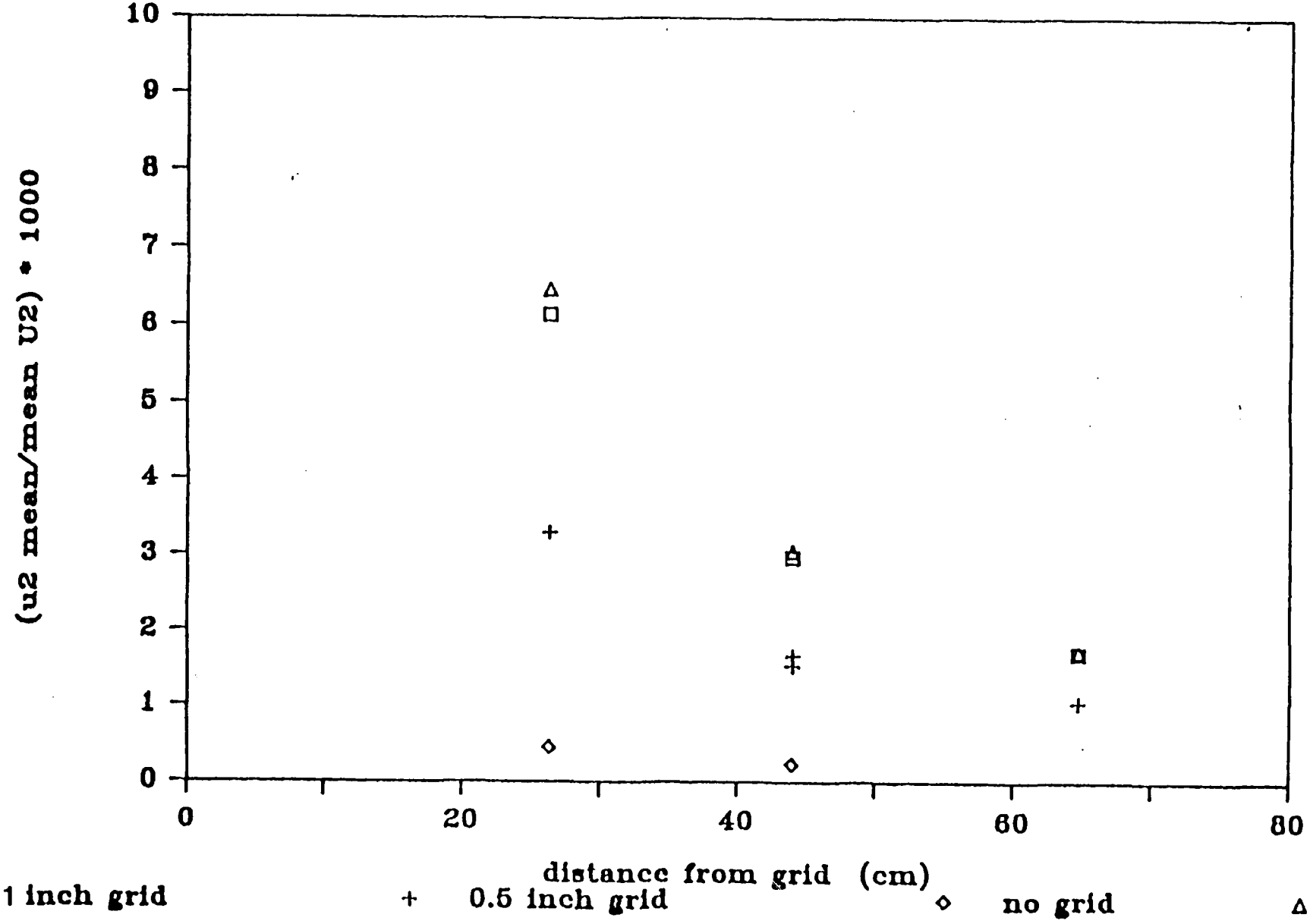

mean square vel/mean vel squared *1000

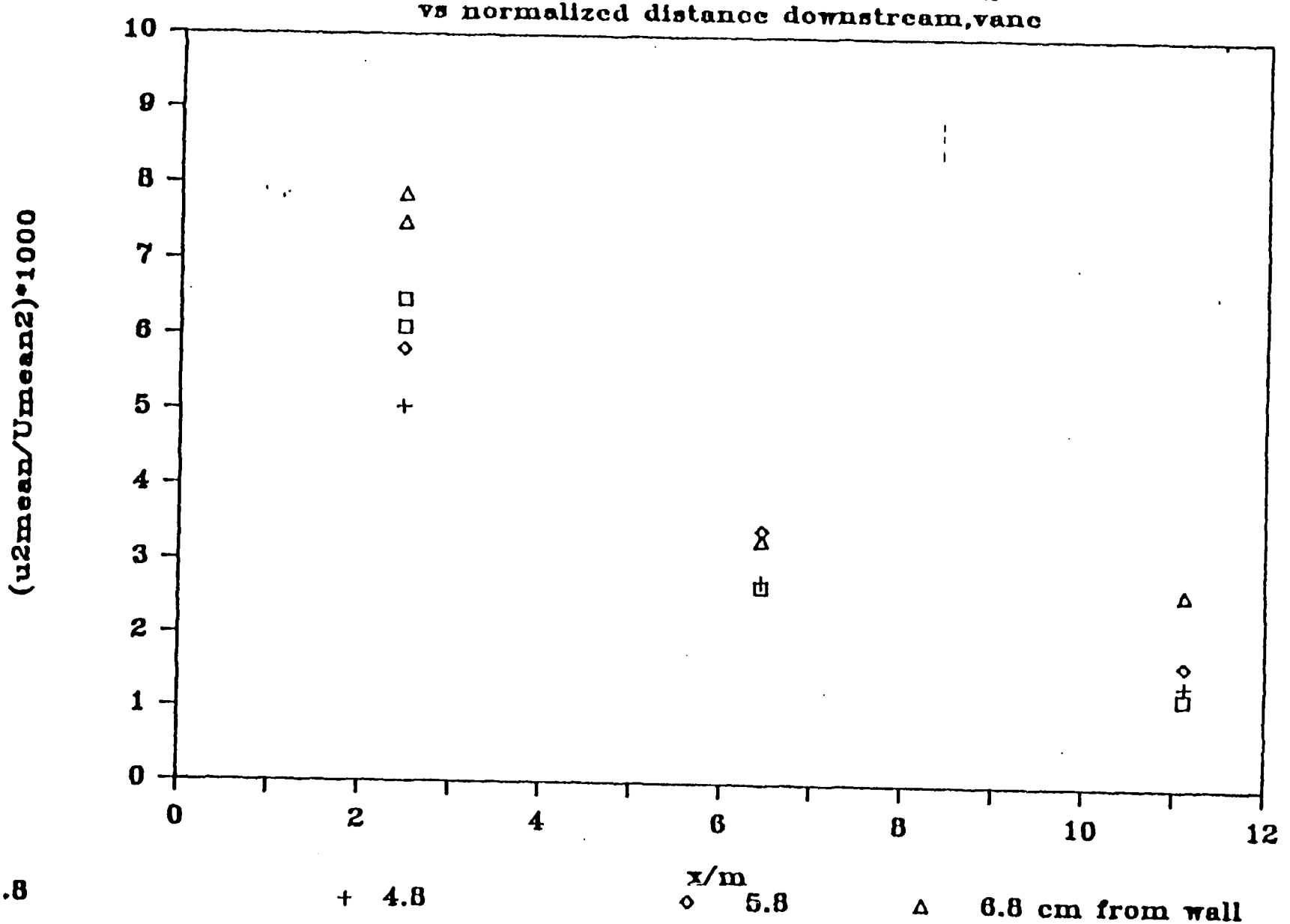

turbulent intensity as motor rpm varies

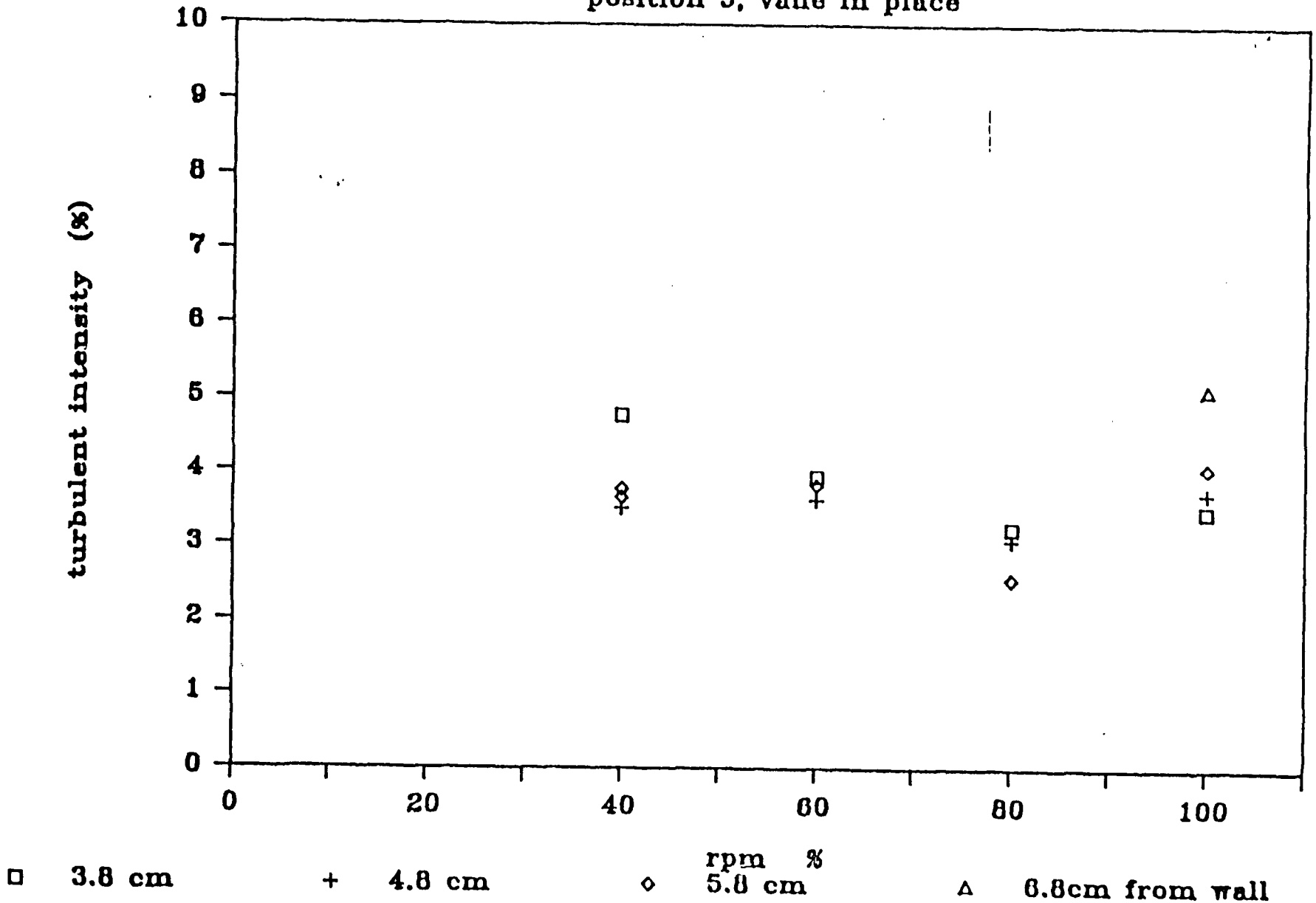

velocities in core as motor rpm varies

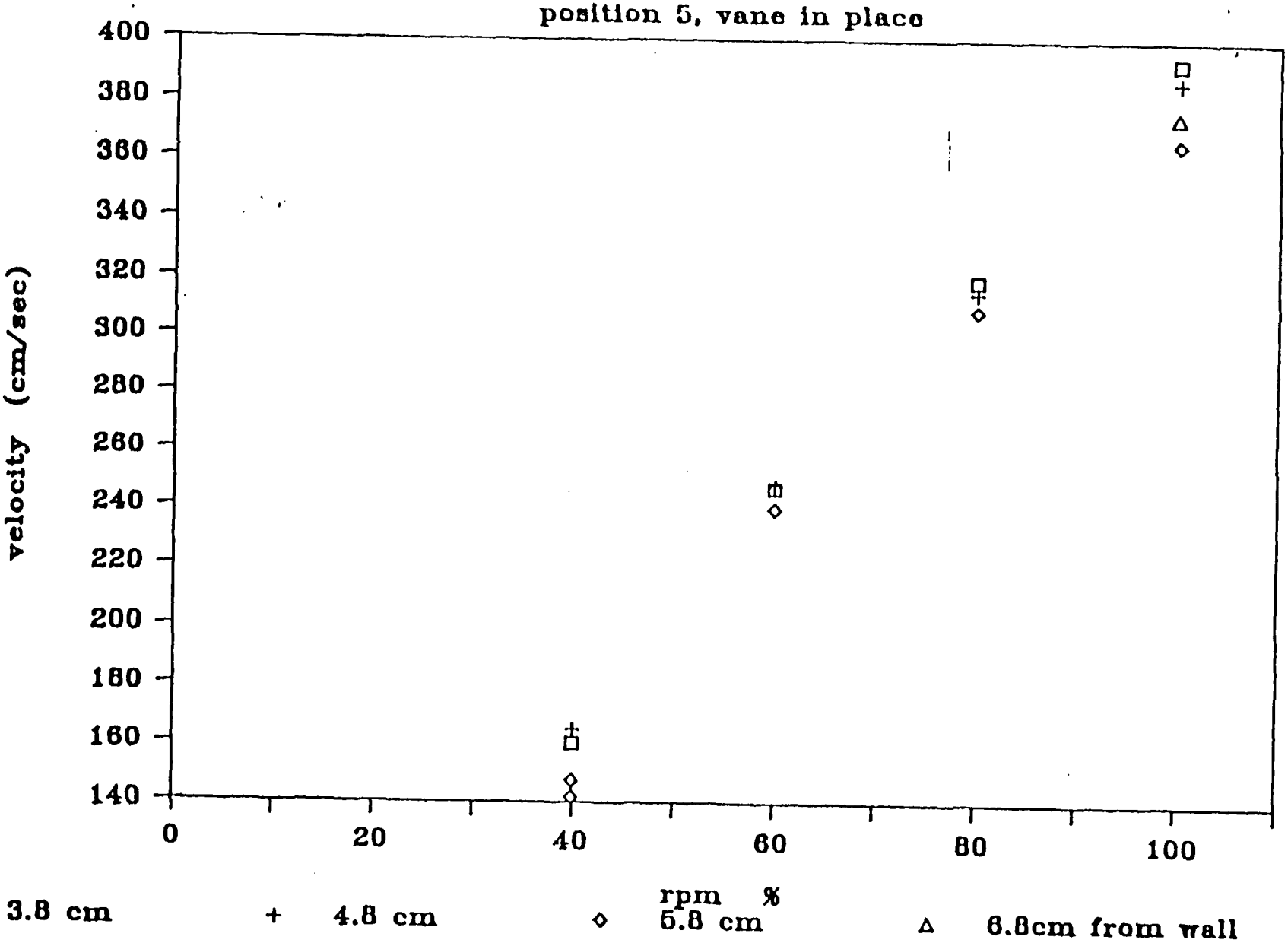

turbulent kinetic energy as motor rpm

varies, position 5, vane in place

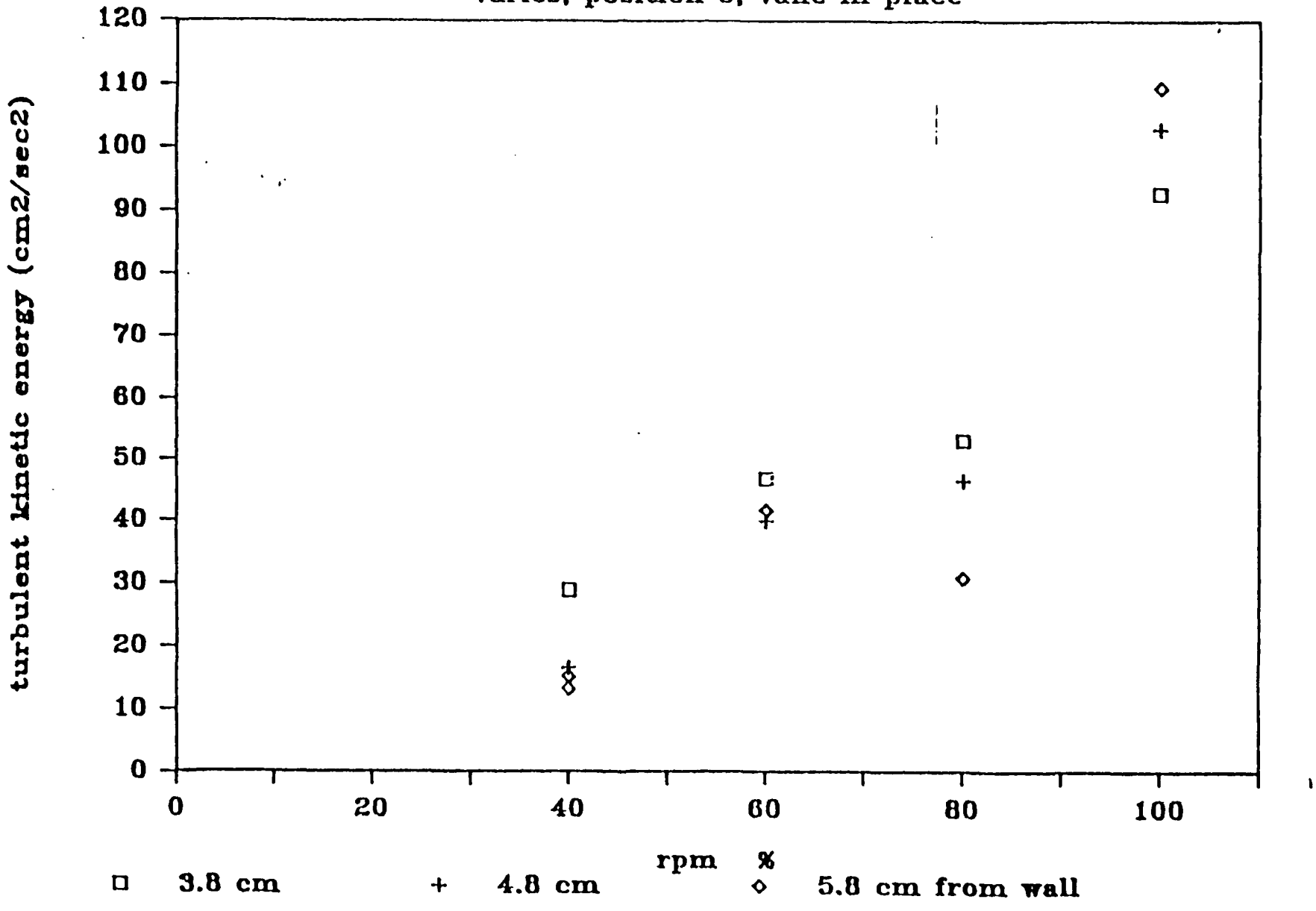

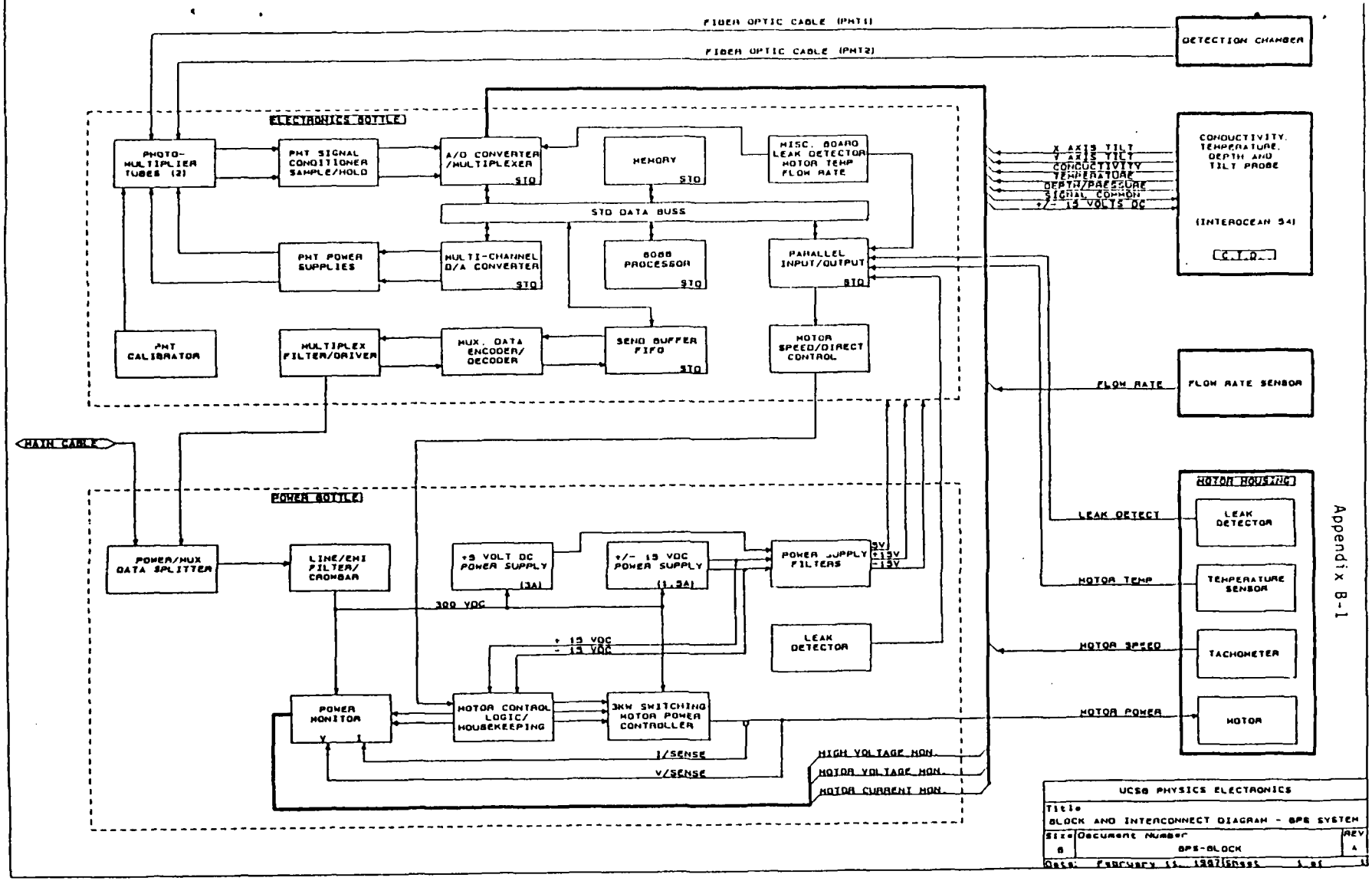
FIBER OPTIC CABLE (PHT1)
FIBER OPTIC CABLE (PHT2)
DETECTION CHAMBER
ELECTRONICS BOTTLE
PHOTO-MULTIPLIER TUBES (2)
PHT SIGNAL CONDITIONER SAMPLE/HOLD
A/D CONVERTER /MULTIPLEXER
STD
MEMORY
STD
MISC. BOARD LEAK DETECTOR MOTOR TEMP FLOW RATE
STD DATA BUSS
PHT POWER SUPPLIES
MULTI-CHANNEL D/A CONVERTER
STD
8088 PROCESSOR
STD
PARALLEL INPUT/OUTPUT
STD
PHT CALIBRATOR
MULTIPLEX FILTER/DRIVER
MUX. DATA ENCODER/ DECODER
SEND BUFFER FIFO
STD
MOTOR SPEED/DIRECT CONTROL
X AXIS TILT
Y AXIS TILT
CONDUCTIVITY
TEMPERATURE
DEPTH/PRESSURE
SIGNAL COMMON
+/- 15 VOLTS DC
CONDUCTIVITY, TEMPERATURE, DEPTH AND TILT PROBE
(INTEROCEAN S4)
C.T.D.
FLOW RATE
FLOW RATE SENSOR
MAIN CABLE
POWER BOTTLE
POWER/MUX DATA SPLITTER
LINE/EMI FILTER/ CROWBAR
+5 VOLT DC POWER SUPPLY
(3A)
+/- 15 VDC POWER SUPPLY
(1.5A)
POWER SUPPLY FILTERS
+5V
+15V
-15V
300 VDC
+ 15 VDC
- 15 VDC
LEAK DETECTOR
POWER MONITOR
V
I
MOTOR CONTROL LOGIC/ HOUSEKEEPING
3KW SWITCHING MOTOR POWER CONTROLLER
I/SENSE
V/SENSE
HIGH VOLTAGE MON.
MOTOR VOLTAGE MON.
MOTOR CURRENT MON.
MOTOR HOUSING
LEAK DETECT
LEAK DETECTOR
MOTOR TEMP
TEMPERATURE SENSOR
MOTOR SPEED
TACHOMETER
MOTOR POWER
MOTOR
UCSD PHYSICS ELECTRONICS
Title
BLOCK AND INTERCONNECT DIAGRAM - BPS SYSTEM
Size
B
Document Number
BPS-BLOCK
REV
A
Date: February 11, 1987
Sheet 1 of 1

Appendix B-1

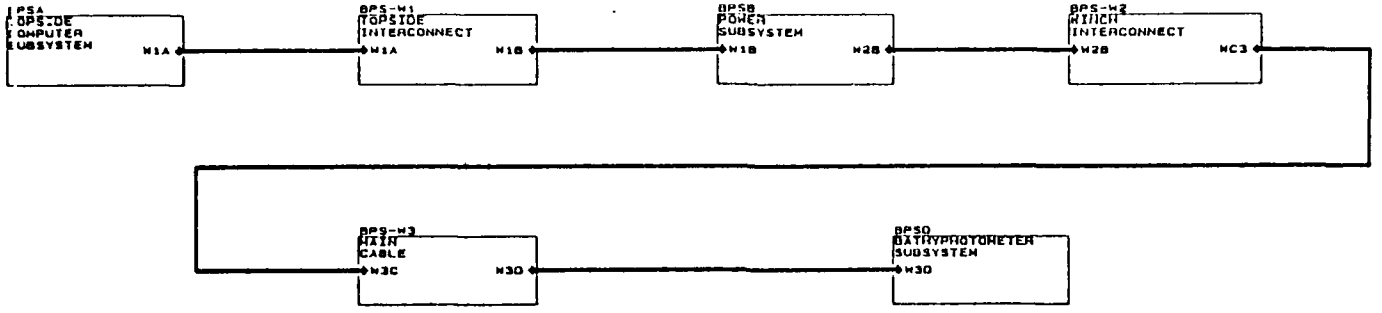

UCSB PHYSICS ELECTRONICS SHOP		
Title: BPS BLOCK DIAGRAM		
Size: B	Document Number: BPS-10L	REV
Date: February 12, 1988	Sheet of	

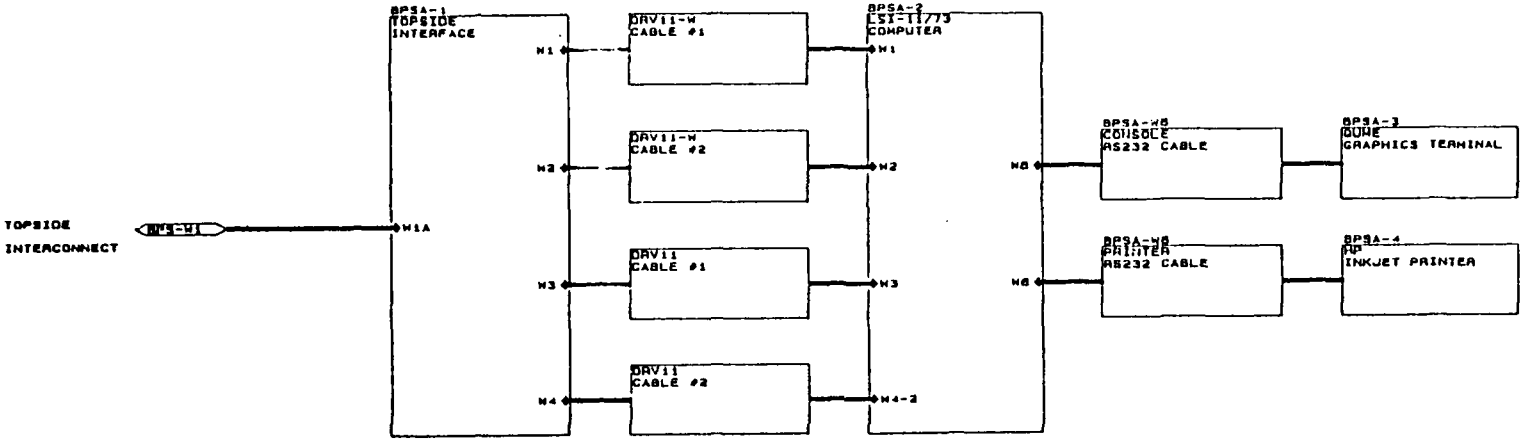

UCSB PHYSICS ELECTRONICS SHOP

Title
TOPSIDE COMPUTER SUBSYSTEM BLOCK DIAGRAM

Size	Document Number	REV
B	BPSA-1BL	

Date: January 11, 1987 Sheet of

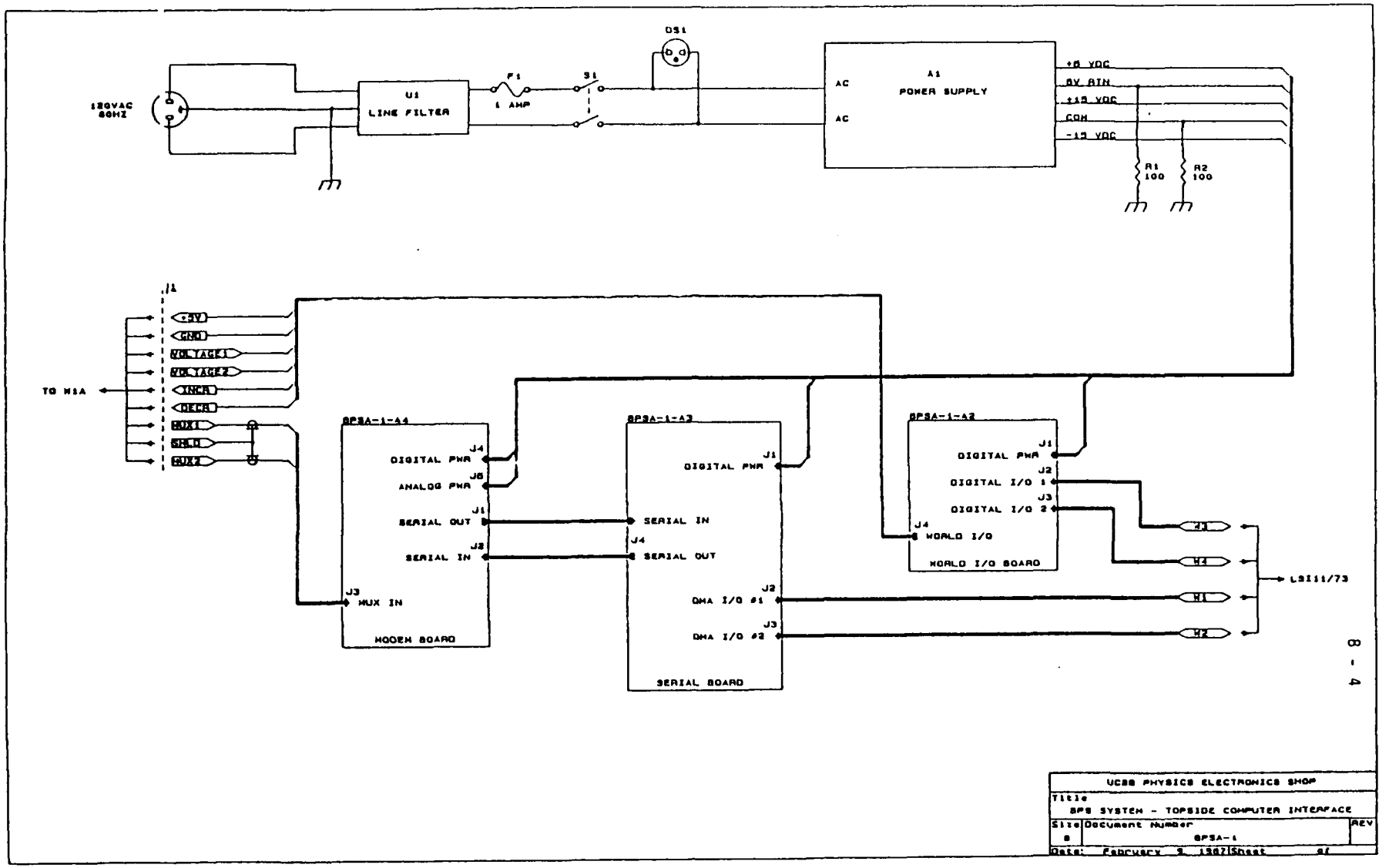

UCSB PHYSICS ELECTRONICS SHOP		
Title: BPS SYSTEM - TOPSIDE COMPUTER INTERFACE		
Size: B	Document Number: BPSA-1	REV
Date: February 9, 1987	Sheet of	

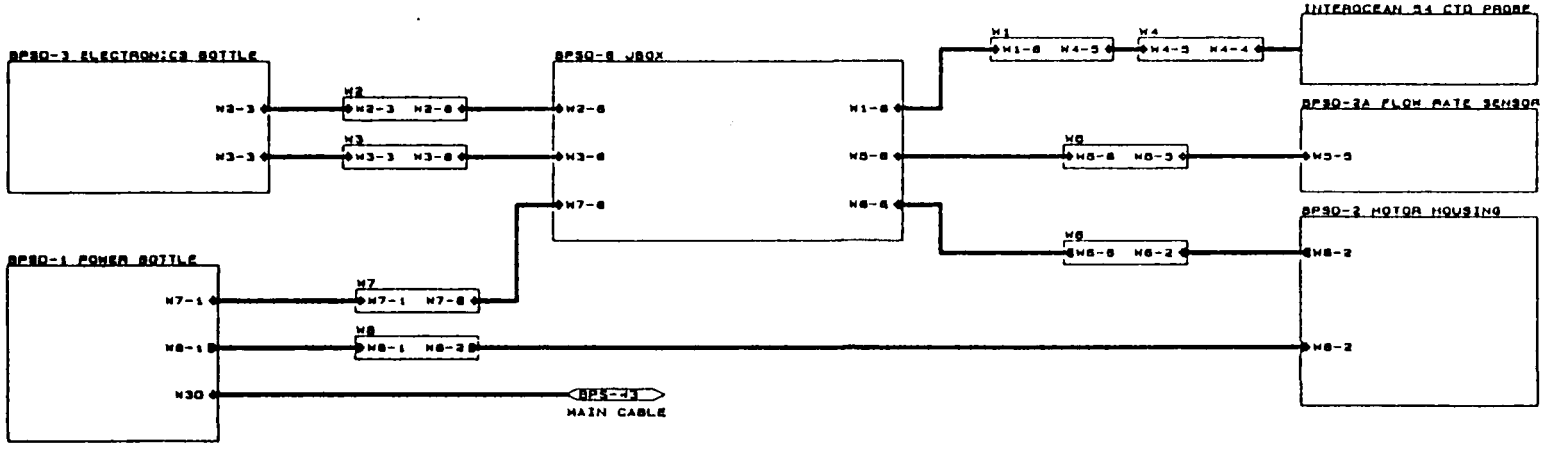

UCSB PHYSICS ELECTRONICS SHOP		
Title: BATHYPHOTOMETER SUBSYSTEM BLOCK DIAGRAM		
Size: B	Document Number: BP3D-18L	REV
Date: February 10, 1987	Sheet of	